Contrib Mineral Petrol (2006) 151: 521–538
DOI 10.1007/s00410-006-0074-7

ORIGINAL PAPER

Jean-Pierre Lorand · Michel Grégoire

Petrogenesis of base metal sulphide assemblages of some peridotites from the Kaapvaal craton (South Africa)

Received: 27 October 2005 / Accepted: 15 January 2006 / Published online: 25 March 2006

Abstract Thirty-two peridotite xenoliths from kimberlitic pipes of the Kaapvaal craton were analysed for S and studied in reflected light microscopy and electron microprobe. Correlation between whole-rock S concentrations and sulphide modal abundances has been obscured by kimberlite-related sulphur within the mantle and by low-temperature contamination processes during emplacement. Mantle-derived base metal sulphides (BMS) occur as solitary inclusions (SI) and intergranular blebs. Unfractured SI encloses intergrowths of Ni-poor and Ni-rich monosulphide solid solution (Mss) phases, coexisting with pentlandite (Pn) and Cu-rich sulphides. Textural relationships between Mss phases and Cu-sulphides are consistent with fractional crystallization of Mss from a Cu–Fe–Ni sulphide melt. Pn-rich euhedral SI may have crystallized from a more metal-rich sulphide melt. However, the opaque mineral assemblages of both fractured sulphide inclusions and intergranular BMS point to a progressive desulphurization of Mss, yielding Pn-rich grains, often replaced by Fe-poor heazlewoodite and abundant magnetite, while Cu-sulphides are replaced by native copper. This trend is consistent with reducing conditions generated by low-temperature serpentinization. A residual origin cannot be ruled out for the Mss enclosed in the most refractory peridotites, although their Ni/Fe ratios are too low to be consistent with an equilibration with olivine at magmatic temperatures. Modal abundances of mantle-derived BMS increase in the Fe-enriched metasomatized peridotites. At least two BMS precipitation processes can be recognized: (1) precipitation of Fe–Cu-rich immiscible sulphide melts in phlogopite-(ilmenite–rutile) peridotites and (2) sulphidation reactions from an H_2S-rich fluid phase in phlogopite-K richterite peridotites.

Electronic Supplementary Material Supplementary material is available for this article at http://dx.doi.org/10.1007/s00410-006-0074-7 and is accessible for authorized users.

Communicated by T. L. Grove

J.-P. Lorand
MNHN USM 201 and CNRS UMR 7160, Minéralogie-Pétrologie, Département "Histoire de la Terre", Muséum National d'Histoire Naturelle, CP 52, 61 Rue Buffon, 75005, Paris, France
E-mail: jplorand@mnhn.fr
Tel.: +33-1-40793522
Fax: +33-1-40793876

M. Grégoire (✉)
Laboratoire Dynamique Terrestre et Planétaire, CNRS-UMR 5562, Observatoire Midi-Pyrénées, Université Paul Sabatier, 14 Avenue E. Belin, 31400, Toulouse, France
E-mail: Michel.Gregoire@dtp.obs-mip.fr

Introduction

Cu–Fe–Ni sulphides [often referred to as base metal sulphides (BMS)] are widespread microphases in mantle-derived rocks (e.g. Lorand and Conquéré 1983; Dromgoole and Pasteris 1987; Lorand 1989a; Guo et al. 1999; Luguet et al. 2003), diamonds (Gurney 1989; Bulanova et al. 1996), basalt-hosted megacrysts (Andersen et al. 1987; Shaw 1997) and xenocrystic minerals (i.e. olivine) from kimberlites (Griffin et al. 2002). Sulphide petrology is relevant to the oxygen and sulphur fugacities of the upper mantle (Eggler and Lorand 1993), to the solid/melt partitioning behaviour of S in mantle melting processes (Morgan 1986; Lorand 1989b) and to mantle metasomatism because S can be mobilized by a wide range of metasomatic agents, from supercritical fluids to volatile-rich alkaline small-volume melts and basalts (Harte et al. 1975; Lorand et al. 2003, 2004).

Sulphide microphases concentrate highly siderophile elements (HSE), i.e. the platinum-group elements (PGEs), as well as Re and Au (Pattou et al. 1996; Alard et al. 2000). Sulphides, therefore, offer the greatest potential for reliable Re–Os dating of mantle processes (Alard et al. 2002). Since pioneering works in the 1970s (i.e. Desborough and Czamanske 1973; Frick 1973; Meyer and Boctor 1975; Tsai et al. 1979), BMS in kimberlite-hosted mantle xenoliths and xenocrysts were mostly investigated as part of more comprehensive studies of Re–Os isotope systematics. Griffin et al. (2002) and Aulbach et al. (2004) in olivine xenocrysts from respectively the Siberian Craton and the Slave Craton (Canada), and Griffin et al. (2004) in peridotite xenoliths from Kaapvaal craton (South Africa) provided compelling evidence for the occurrence of several generations of sulphides (sometimes together inside a single olivine xenocryst) yielding a wide range of Re-depletion ages (3.5–0.5 Ga). The present study, based on reflected light microscopy and electron microprobe studies of 32 samples of mantle peridotites from the Kaapvaal craton, focuses on the crystallization/recrystallization history of the BMS, especially with respect to redox conditions imposed by non-sulphide major minerals. Kimberlite-hosted peridotite xenoliths are generally more serpentinized than basalt-hosted peridotites; thus, their BMS parageneses should reflect this higher degree of alteration (e.g. Lorand 1985, 1989a). Finally, the origin (metasomatic vs residual) and the precipitation mechanism of the various BMS generations are distinguished on the basis of mineralogical, textural and chemical criteria.

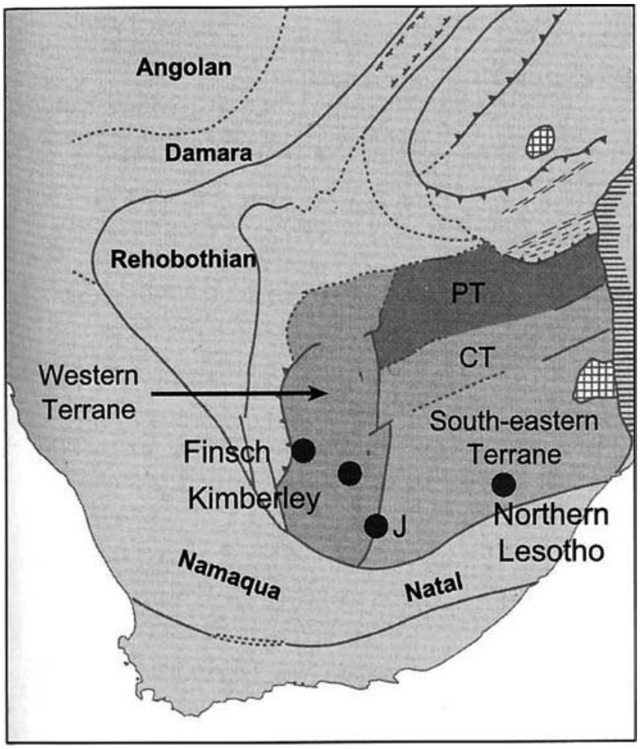

Fig. 1 Schematic geological map of the Kaapvaal craton showing the studied kimberlite localities (after Griffin et al. 2003a); *K* Kimberley (Premier Mine, De Beers); *J* Jagersfontein; Northern Lesotho (Thaba Putsoa; Matsoku; Mothae; Liqhobong). For more detail, see text

Sampling and analytical methods

The Kaapvaal craton is interpreted as a late Archean collage of four low- to high-grade Archean Terranes: the Western Terrane, the South-Eastern Terrane, the Central Terrane and the Pietermaritz Terrane (de Wit et al. 1992; Griffin et al. (2003a, b). In the Western Terrane, xenoliths come from the diamondiferous kimberlite pipes of the Kimberley area (De Beers Mine; Bultfontein, Kimberley, South Africa) and Jagersfontein (Fig. 1). In the South-Eastern Terrane, samples come from several diamondiferous kimberlite localities from Northern Lesotho (Matsoku, Thaba Putsoa, Mothae and Liqhobong). The Kimberley samples belong to the rock collection of the Natural History Museum, Paris. The other samples were obtained from the Department of Tectonophysics, University of Montpellier, France. The main textural, geochemical and petrological features of Kaapvaal xenoliths are summarized in several review papers (e.g. Boyd and Nixon 1978; Boyd and Gurney 1986; Nixon 1987; Boyd 1989). Those of Jagersfontein and Bultfontein samples are available in Hops et al. (1989), Dawson et al. (1980), Erlank et al. (1987) and Field and Haggerty (1994).

The studied mantle xenoliths from Kimberley and Jagersfontein localities are mostly coarse-granular depleted peridotites, which are the dominant lithology of the continental lithospheric mantle at depths between 120 and 170 km (Griffin et al. 2003a). Coarse-grained textures are characterized by grains up to several centimetres in length; several samples show evidence of incipient recrystallization marked by small ($<<100$ μm across) olivine neoblasts. Bultfontein and Jagersfontein coarse-grained samples show well-developed serpentine network (± calcite ± brucite), representing up to 20% by volume of the host sample. Both garnet-bearing and garnet-free peridotites occur in our Bultfontein and Jagersfontein collection of samples. The garnet peridotites are always lherzolites, i.e. they display at least one clinopyroxene crystal in thin section (Boyd and Nixon 1978). Garnet compositions plot in the lherzolitic field of the CaO vs Cr_2O_3 diagram of Sobolev et al. (1973). The *P*–*T* conditions of eight samples were determined from electron microprobe analyses (CAMECA SX 50 facility, CAMPARIS, Paris; Lorand unpublished data), using the geothermometers garnet–orthopyroxene of Harley (1984) and Ca-in-orthopyroxene of Brey and Kohler (1990) and the Taylor (1998) geobarometer. The results ($950 < T < 1{,}000$°C; $4.0 < P < 4.3$ GPa; Table 1) are consistent with an equilibration on a low-heat flow cratonic geotherm, while the narrow range of pressure suggests a provenance from a restricted depth window (110–130 km).

Garnet-free peridotites are chromite-bearing harzburgites and lherzolites; the samples from Jagersfontein and Bultfontein contain delicate symplectites of Cr-spinel + clinopyroxene ± Al–Cr–Ca-poor enstatite. These symplectites have been interpreted as products of stress-assisted decompression affecting Al–Cr–Ca-rich clinoenstatite, which occurred prior to or during protokimberlite genesis and sampling (Field and Haggerty 1994). Olivine is always corroded by this symplectitic association. Mean forsterite (Fo) contents of

Table 1 Key petrographic features of the studied samples

Sample	Locality	Texture	Rock-type	Fo (%)	En (%)	T(°C-HA84)	T(°C-BK90)	P(GPa-T98)	Metasomatic minerals	Hydrothermal minerals
Western Terrane										
Garnet-free peridotites										
Jagersfon (S)	Jagersfontein	Coarse-granular	Lherzolite[a]	93.0	93.7					
KBBJ	Jagersfontein	Coarse-granular	Harzburgite[b]	92.5	91.4					
Jagersfon 1	Jagersfontein	Coarse-granular	Harzburgite[a]	n.a.	n.a.					
Bult. 9	Bultfontein	Coarse-granular	Harzburgite[b]	92.7	91.4					
Bult. 17	Bultfontein	Coarse-granular	Harzburgite[b]	92.7	92.2					
Bult. 8 (S)	Bultfontein	Coarse-granular	Lherzolite[b]	92.5	91.6					
Bult. 4 (S)	Bultfontein	Coarse-granular	Lherzolite[b]	91.5	92					Brucite
Garnet peridotites										
Bult. 15	Bultfontein	Coarse-granular	Lherzolite	93.3	93.5					
Bult. 11	Bultfontein	Coarse-granular	Lherzolite	93.1	93.2	1,003 ± 12	988 ± 8.5	4.1 ± 0.8		Calcite
Bult. 3 (S)	Bultfontein	Coarse-granular	Lherzolite	93.2	93.3	978 ± 31	985 ± 7	4.1 ± 0.8		
Bult. 7	Bultfontein	Coarse-granular	Lherzolite	n.a.	n.a.					
Bult. 17′	Bultfontein	Coarse-granular	Lherzolite	n.a.	n.a.	1,000	982	4.1		
Bult. 2	Bultfontein	Coarse-granular	Lherzolite	n.a.	n.a.					
80 191	Bultfontein	Coarse-granular	Lherzolite	n.a.	n.a.	990	962	4.0	Phlogopite	
80 192	Bultfontein	Coarse-granular		92.7	93	960	991	4.2		
KBD 4 (S)	De Beers mine	Porphyroclastic	Harzburgite	92.9	93	975	969	3.7		
BG2 (S)	Kimberley mine	Coarse-granular	Harzburgite	93	93	960	967	3.9	Phlogopite	Calcite
BG (S)	Kimberley mine	Porphyroclastic	Lherzolite	92.0	92.4	979	1,008	4.1	Phlogopite	
Phlogopite K-richterite peridotites (PKP)										
Bult. 1	Bultfontein	Coarse-granular	Lherzolite	n.a.	n.a.				Phlogopite	
Bult. 16	Bultfontein	Coarse-granular	Lherzolite	n.a.	n.a.				+ K-richterite	
Bult. 6 (S)	Bultfontein	Coarse-granular	Lherzolite	90	91.8				+ CpxII	
Bult. 12	Bultfontein	Coarse-granular	Lherzolite	91.8	92.5					
South-Eastern Terrane										
Garnet-free peridotites										
LTP 20	Thaba putsoa	Coarse-granular	Lherzolite[a]	93.4	93.7				CpxII + chromite	
PHN 1914b	Mothae	Coarse-granular	Lherzolite[a]	93.0	92.8					
Garnet peridotites										
PHN 1569	Thaba putsoa	Coarse-granular	Lherzolite[a]	92.5	93.2	860	930	3.6	Phlogopite	
PHN 1914a	Mothae	Coarse-granular	Lherzolite	92.2	93.1	854	872	3.3		
LMT 2 (S)	Mothae	Coarse-granular	Lherzolite	92.7	93.4	924	997	4.2		
LMT 1	Mothae	Coarse-granular	Lherzolite	91.5	92.1				Phlogopite	
KBM 39	Mothae	Granuloblastic	Lherzolite	88.9	89.0	973 ± 30	1,004 ± 17	3.5	Ilmenite–rutile–phlogopite	
LLQ 2	Liqhobong	Granuloblastic	Harzburgite[a]	92.7	93.7	980	1,013	3.8	Phlogopite	
PHN 2899	Liqhobong	Granuloblastic	Lherzolite	91.4	90					
LMA 2	Matsoku	Granuloblastic	Lherzolite	93.7	93	960	986	3.6	Phlogopite	
LMA 7	Matsoku	Granuloblastic	Lherzolite	92.2	93.0	960 ± 32	979 ± 5	3.6 ± 0.8		
LMA 18	Matsoku	Granular	Lherzolite[a]	91.6	92	1,012 ± 29	1,005 ± 15	3.7 ± 0.12	Phlogopite	

Fo Olivine Fo percentage, *En* Orthopyroxene enstatite percentage, *n.a.* not analysed, *Ol* Olivine, *Op*x orthopyroxene, *Cpx* clinopyroxene, *Cr Sp* Chrome spinel, *S* Strongest degree of serpentinization (does not exceed 20–30 vol%)

HA84 Harley (1984), BK90 Brey and Kohler (1990) and T98 Taylor (1998)

[a] Euhedral chromite

[b] Chromite-pyroxene intergrowths

harzburgitic and lherzolitic olivine range from 91.5 to 93.7, i.e. within the range previously reported for similar rocks (Griffin et al. 2003a, b and reference therein). An obvious modal metasomatic feature is the ubiquitous occurrence of phlogopite. Four Bultfontein samples contain the assemblage Ti-phlogopite, K-richterite, ilmenite, armalcolite and titanate-like phases referred to as garnet–phlogopite (GPP) and phlogopite K-richterite peridotites (PKP; Erlank et al. 1987). The metasomatic phases are considered to be crystallization products from LILE-enriched fluids, possibly related to the MARID suite and predating the kimberlitic extrusion by less than 100 Ma (Kinny et al. 1993; Grégoire et al. 2002, 2003). K-Richterite, armalcolite and lindsleyite (a titanate) assemblages are stable between 900 and 1,100°C for pressure ranging between 2 and 3 GPa (see Haggerty 1989, 1991, for more details).

The South-Eastern Terrane xenoliths are coarse-grained chromite-bearing lherzolites (e.g. LTP 20) or coarse-grained garnet lherzolites (e.g. PHN 1562; Table 1), showing a restricted range of olivine compositions (Fo: 92.2–93.4). Depleted mantle peridotites beneath Northern Lesotho erupted from a narrow window of the SCLM (120–170 km; Griffin et al. 2003a). The P–T conditions determined for eigth garnet-bearing samples (Table 1) show that our samples come from the uppermost part of this window ($930 < T < 1{,}020$°C; $3.5 < P < 3.8$ GPa; Table 1). These P–T conditions agree well with those previously determined for similar Matsoku xenoliths (e.g. Gurney et al. 1975; Harte et al. 1987). Samples LMA 2, LMA 7, LMA 18 and KBM 39 differ by porphyroclastic or mosaic porphyroclastic to granuloblastic microstructures characterized by abundant triple junctions at 120° and a lower grain size (< 1 mm). That recrystallization process is associated with metasomatism by Fe–Ti alkali melts (Harte et al. 1987). LMA 7 and LMA 18 (Matsoku), two garnet–clinopyroxene-rich lherzolites with abundant phlogopite, have olivine characterized by relatively low Fo contents (92.2–91.6). KBM 39, a Mothae pyroxene-rich peridotite sample, is enriched in Fe (Fo 88.9) and Ti, related to the numerous ilmenite ± rutile inclusions in olivine and garnet and the abundance of primary phlogopite (5% by volume).

Analytical methods

Western Terranes xenoliths were studied in reflected light microscopy using two to six polished thin sections per sample. By contrast, only one or two thin sections were available for the South-Eastern Terrane xenoliths. Sulphide modal abundances were determined by image analysis from digitized plane-polarized reflected light microphotographs of polished thin section at magnification ×20, using a digital Olympus DP-10 camera adapted on an Olympus BX60 microscope connected to a PC. Each microphotograph integrated a surface of about 4×3.2 mm^2 in size (i.e. 1,280×1,024 pixels). Thus, the complete picture of each polished thin section (3–10 cm^2) required several photomicrographs assembled together by using the application software, PanaVue Image Assembler. The total surface area occupied by sulphide grains was estimated using the Adobe Photoshop software, using its colour range selection tool for sulphide grains more than ca 20×20 μm^2 in maximum size and a grain-by-grain selection for the smallest sulphide grains. The grain size detection limit of the method was defined by pixel sizes (3.1×3.1 μm^2). Analytical error on total surface area occupied by sulphide grains is about 10%. This latter value takes into account the microphotograph quality and optical artefacts resulting from colour overlapping between sulphide and serpentinization-related magnetite (Mt).

Bulk-rock S concentrations of 23 samples were determined by iodometry of the SO_2 produced by combustion at 950°C of 500 mg powder aliquots (prepared from 1 kg rock chip). The two international rock standards analysed in this study, SY2, a CANMET syenite and JP1, a peridotite, give S contents in excellent agreement with the recommended values (Lorand et al. 2003; Gros et al. 2005).

BMS and native metals have been analysed with a fully automated CAMEBAX electron microprobe at the National Natural History Museum (Paris). The analytical conditions were 15 kV acceleration voltage, 10 nA current beam and 10 s/peak, 10 s/standard counting times. Ni, Co, Cu have been determined with pure metal internal standards, while a natural pyrite was used for Fe and S. In order to discuss Ni–Fe partitioning between olivine and sulphides, Ni has been analysed in olivine with a special procedure coupling a longer counting time (40 s/peak, 40 s/background) and a 25 kV acceleration voltage.

BMS occurrences and modal abundances of mantle-derived sulphides

Basically four types of sulphide occurrence can be defined in Kaapvaal peridotite xenoliths, in agreement with previous studies (e.g. Frick 1973; Griffin et al. 2004).

(1) Large (up to 250 μm in diameter), rounded to euhedral single sulphide blebs isolated in silicates, and unrelated to fracture planes (Fig. 2a). A silicate crystal commonly contains only one of such large sulphide inclusion; they will therefore be referred to as single sulphide inclusions (SI). These inclusions are commonly surrounded by fracture planes, which may or may not communicate with the grain boundaries of host silicates. This kind of fracture system is generally assumed to result from a volume increase of enclosed sulphides during cooling (Andersen et al. 1987; Dromgoole and Pasteris 1987). These fracture planes are preferential pathways for serpentinization.

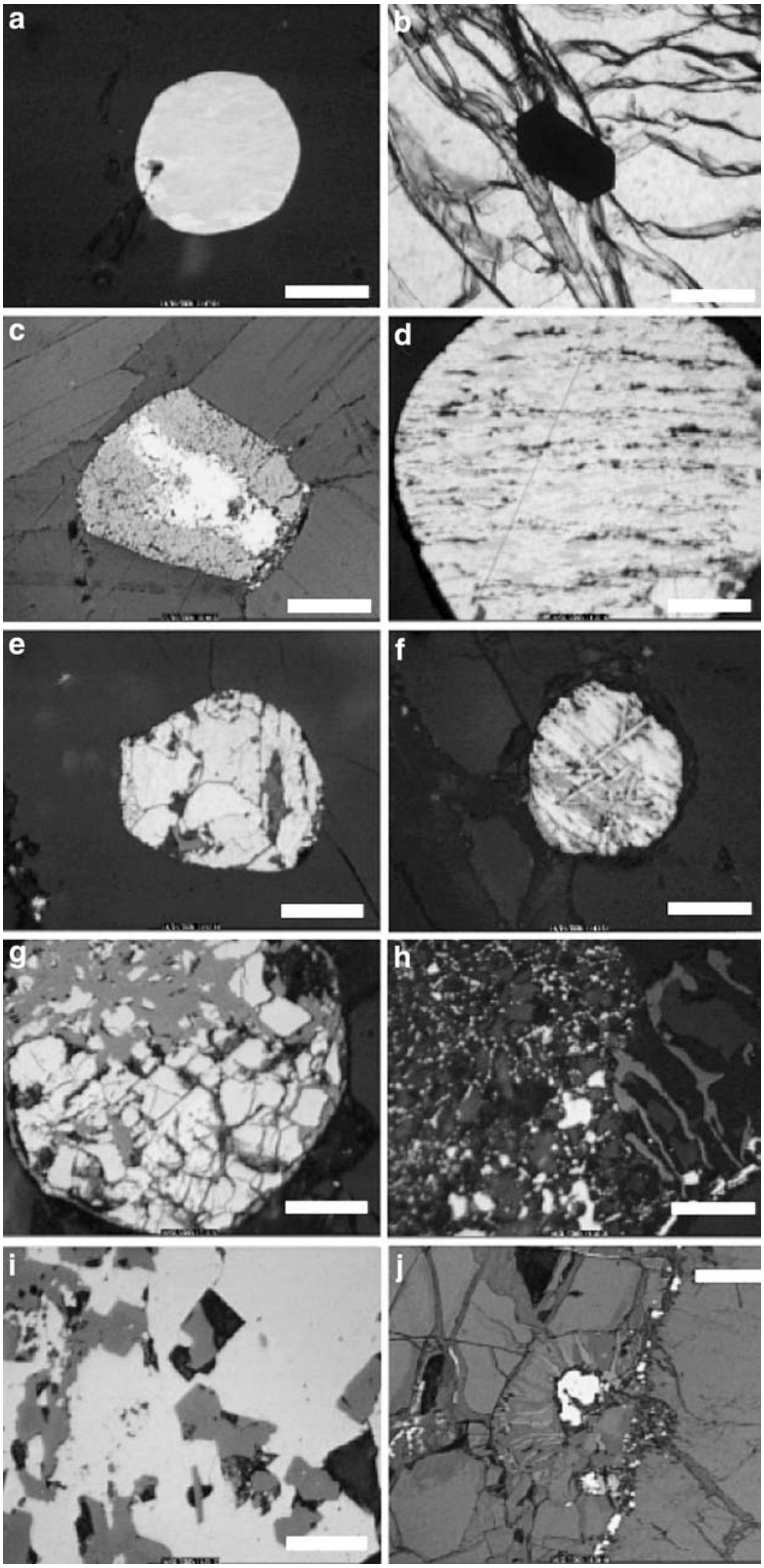

Fig. 2 Microphotographs of base metal sulphides (*BMS*) and other Cu–Fe–Ni opaque minerals in Kaapvaal peridotites (plane-polarized reflected light except Fig. 2b, plane-polarized transmitted light). **a** single sulphide inclusion in olivine; note the finely intergrown Mss phases; *white patches* are Pn. Sample LMA 18; *scale bar* = 50 µm. **b** single sulphide inclusion in olivine with hexagonal cross-section. Sample Bult. 15; *scale bar* = 100 µm. **c** intergranular sulphide (Hz + Pn) partly replaced by Mt in PKP sample Bult. 12; note the phlogopite crystals surrounding the BMS. *Scale bar* = 200 µm. *PKP* Phlogopite-K-richterite peridotites. **d** two-phases (Pn + Cp) rounded BMS inclusion in Opx. Sample KBM 39; *scale bar* = 30 µm. **e** enlargement of a Pn–Mss intergrowth from a fractured BMS inclusion; note the coarse Pn bodies at the lower right corner. Sample Bult. 3; *scale bar* = 20 µm. **f** single SI displaying rod-like Pn exsolutions cross-cutting a fine intergrowth of Pn + pyrrhotite; incipient weathering is indicated by *greyish iron hydroxides*. Samples 80–191; *scale bar* = 50 µm. **g** polyhedral BMS inclusion in serpentinized olivine, totally recrystallized into Fe-rich Pn (*light grey*), Mt (*dark grey*) and native copper (*Cu*). Sample Bult. 6; *scale bar* = 20 µm. **h** clusters of BMS micrograins scattered in a Cpx + Cr-spinel symplectite. Sample KBBJ. *Scale bar* = 10 µm. **i** euhedral Mt (*dark grey*) inclusions in a polycrystalline Hz. Sample Bult. 4; *scale bar* = 20 µm. **j** native nickel grain (*bright*) in the core of a Cr-spinel + pyroxene symplectite. Sample Bult. 4; *scale bar* = 100 µm

(2) Trails of SI composed of small-sized (1–20 µm radius) sulphide droplets located within the fracture planes radiating from SI; similar small spherical SI were occasionally observed in olivine neoblasts located around large interstitial sulphide blebs.

(3) Interstitial sulphide blebs: they are euhedral to anhedral sulphide bodies, up to 300×400 μm in maximum size, disseminated within the silicate matrix. Some of them display nearly perfect hexagonal cross-sections while other are rounded or polyhedral. True intergranular sulphides and SI completely coated by serpentine can be distinguished in cross-polarized transmitted light only.

(4) Clusters of sulphide grains intergrown with Cr-spinel + clinopyroxene ± enstatite symplectites in Jagersfontein and Bultfontein garnet-free peridotites. Thin (<20 μm) sulphide veinlets up to several millimeters in length are associated to such clusters, being exclusively located within grain boundaries or fracture planes of olivine.

Unlike type 4, BMS types of occurrence 1–3 have been widely described in peridotite xenoliths and interpreted as mantle-derived (e.g. Frick 1973; Lorand and Conquéré 1983; Dromgoole and Pasteris 1987; Guo et al. 1999; Griffin et al. 2004). Modal abundance of such mantle-derived BMS shows a broadly negative correlation with olivine compositions (Fig. 3). Apart from one sample (LLQ2), refractory peridotites characterized by Fo content of olivine >92 are nearly devoid of BMS; half of these samples do not contain any BMS (Tables 1 and 2). The less magnesian peridotites (Fo <92) that comprise metasomatized samples (PKP, Fe–Ti-rich peridotites), are richer in BMS (up to 0.08 vol%). This relationship, already reported by Griffin et al. (2004) is observed in Western Terrane xenoliths as well as in South-Eastern Terrane xenoliths.

In the Western Terrane, whether garnet-bearing or not, magnesian peridotites (Fo > ca. 92) are extremely poor in both SI and intergranular sulphides (Table 1). Each polished thin section contains between 0 and 2 olivine-hosted SI. Intergranular sulphides are scarce or almost lacking, even in porphyroclastic samples (KBD4, De Beers Mine). Neither SI nor intergranular sulphide has been found in samples Bult. 4, Bult. 9 (Bultfontein) and BG (Kimberley), which were investigated on the basis of 6, 3 and 4 polished thin sections, respectively. By contrast, only two polished thin sections were necessary to find SI in samples Jagersfon and KBBJ (Jagesfontein; $92.5 < \mathrm{Fo}_{\mathrm{olivine}} < 93.0$). These strong variations reflect a highly heterogeneous distribution of SI and intergranular sulphides in magnesian peridotites. Most SI occur in coarse olivine grains and display hexagonal cross-sections with a maximum size up to 250×120 μm (Fig. 2b). Spherical SI are very rare. Polyhedral SI have also been trapped in orthopyroxene (35% of the total number of SI) and occasionally in clinopyroxene (two inclusions). Pyroxene-hosted SI have negative-crystal shape.

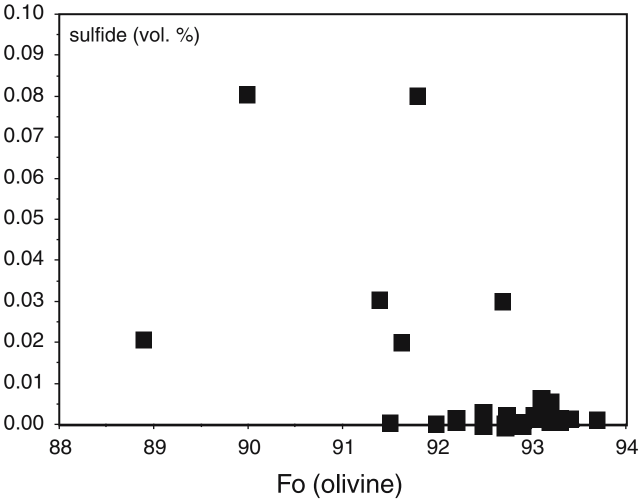

Fig. 3 BMS modal content vs Fo content of the olivine

The two phlogopite-bearing magnesian peridotites (80–191; BG2) contain a few large (up to 400 μm across) hexagonal-shaped sulphides partly enclosed in orthopyroxene. BMS abundance significantly increases in PKP (phlogopite and K-richterite-bearing peridotites) samples, in agreement with previous observations on similar metasomatized peridotites (Erlank et al. 1987). SI occur not only in olivine and orthopyroxene but also in spinel, K-richterite and phlogopite. Intergranular sulphides (up to 17 grains/pts in B6) are intimately associated with phlogopite (Fig. 2c). In some cases, a single polyhedral intergranular sulphide, up to 700×400 μm^2 in size, occurs in the core of polycrystalline phlogopite aggregates. Phlogopite crystals have nucleated on sulphide and enclose small sulphide grains. Conversely, sulphides may form discontinuous rims around the phlogopite. However, PKP are not uniformly enriched in BMS (cf. sample B16; Table 1).

Only 2 polished thin sections, over the 11 polished thin sections investigated in reflected light microscopy, of magnesian peridotites (Fo >92) from the South-Eastern Terrane show olivine-hosted SI, both surrounded by serpentinized fracture planes. Intergranular sulphides are rare and often absent. In Mothae and Thaba Putsoa xenoliths, intergranular sulphides preferentially occur in phlogopite-bearing peridotites (e.g. PHN 1569; LMT 1). The 23 SI occurring in a single thin section of sample KBM 39, the Fe-enriched (Fo 88.9) ilmenite-rutile-phlogopite lherzolite, indicate that this sample is strongly enriched in BMS. These SI are almost equally distributed between olivine (45%) and orthopyroxene (50%). In this sample, clinopyroxene and garnet may also enclose SI and a single orthopyroxene or olivine crystal may enclose up to 3 or 4 SI. In such SI clusters, the inclusions are interconnected by a fracture network, which commonly does not reach the grain margins of the host silicate. Olivine-hosted SI are commonly rounded to regularly faceted and less than 70 μm in diameter. Fluid inclusions may seal radial fracture planes.

In the three studied Matsoku xenoliths, BMS modal proportions increase from the most magnesian peridotite (LMA 2; Fo 93.7), only containing three orthopyroxene-hosted SI, to the less magnesian samples (LMA

7; Fo 92.2) and LMA 18 (Fo 91.6; Table 2). The latter sample, a phlogopite–garnet granular lherzolite is rich in both SI (23 in a single polished thin section) and intergranular sulphides. It shares many features with KBM 39, i.e. SI almost equally distributed between olivine and orthopyroxene, the prismatic (negative crystal) shape of some orthopyroxene-hosted inclusions, clusters of 4–5 SI in a single silicate crystal, inclusions being interconnected by a fracture network sometimes sealed by dark fluid inclusion trails. It only differs from KBM 39 by a higher number of serpentinized fractures and thus some of its olivine-hosted SI are surrounded by serpentine.

Bulk-rock S concentrations

Bulk-rock S concentrations range between 68 and 219 ppm, in agreement with the concentration range

Table 2 Bulk-rock S contents and sulphide occurrences

Sample	S^M (ppm)	Sulphide (vol%)	SI/p.t.s.	Inter. sulphides	Sulphide veins	Additional comments
Western Terrane						
Garnet-free peridotites						
Jagersfon	155	b.d.l.	1/2	-	(+)	Hz in symplectites; native Ni
KBBJ	140	b.d.l	1/2	-	+ +	
Jagersfon 1	150	b.d.l	0/3	((+))	-	
Bult. 9	112	-	0/3	-	-	
Bult. 17	n.a.	b.d.l	1/3	(+)	+	
Bult. 8	n.a.	-	0/3	-	+	Hz (veinlets + coarser grains)
Bult. 4	n.a.	-	0/6	-	+ +	Hz veinlets + native Ni
Garnet peridotites						
Bult. 15	62	b.d.l	0/2	-	-	Opx-hosted SI
Bult. 11	105	0.006	1/4	-	(+)	+ Hz veins, native Cu
Bult. 3	n.a.	0.005	2/3	-	-	Largest (250 μm) SI
Bult. 7	125	b.d.l	1/2	-	-	
Bult. 17′	n.a.	-	1/2	-	(+)	
Bult. 2	93	-	0/1	(+)	-	
80 191	n.a.	0.02	1/2	+	+	Euhedral SI
80 192	n.a.	-	0/2	-	((+))	Hz
KBD 4	215	-	0/1	-	-	
BG2	219	b.d.l	5/6	-	-	
BG	84	-	0/4	-	-	
Phlogopite K-richterite peridotites (PKP)						
Bult. 1	193	0.01 ± 0.005	0/1	+ +	-	Pn–Hz–native Cu
Bult. 16	176	b.d.l	0/1	-	(+)	
Bult. 6	213 (260)	0.08 ± 0.01	2/3	+ +	-	SI in richterite and spinel; native Cu
Bult. 12	182 (167)	0.08	1/4	+ +	+	+ Opx-hosted SI
South-Eastern Terrane						
Garnet-free peridotites						
LTP 20	70	b.d.l	0/3	(+)	-	Inter. sulphides < 30 μm secondary Cu sulph
PHN 1914b	62	b.d.l	1/2	((+))	-	
Garnet peridotites						
PHN 1569	n.a.	b.d.l	0/2	(+)	-	Inter. sulphides < 50 μm
PHN 1914a	53	b.d.l	1/1	(+)	-	Inter. sulphides < 10 μm
LMT 2	n.a	b.d.l	0/1	-	-	
LMT 1	n.a.	b.d.l	0/1	(+)	-	Two grains (< 30 μm)
KBM 39	n.a.	0.02	23/1	+	-	SI in Ol, Opx, Cpx, Gt
LLQ 2	130	0.03	0/1	+	+	Numerous Pn veinlets
PHN 2899	120 (187)	0.03	5/1	+	-	Secondary incl. in Ol. neoblasts
LMA 2	68	b.d.l	0/1	-	-	Opx-hosted SI
LMA 7	132	b.d.l	0/1	+	-	Opx-hosted SI
LMA 18	n.a.	0.02	23/1	+	-	Opx-hosted SI
Rock standards						
SY-2	123					
JP-1	26.5–27					

S^M Measured S content, *Sulphide* (*vol*%) sulphide modal abundance (*b.d.l* below detection limit; ca. 0.001%); *SI*/*p.t.s.* number of solitary sulphide inclusions (*SI*) per standard (2.5×4 cm^2) polished thin section, ((+)) 1 grain per polished thin section, (+) 5–10 grains per polished thin section, + 10–20 grains per polished thin section, + + > 20 grains per polished thin section, *Incl.* enclosed sulphides, *Inter* Intergranular sulphides, *Pn* pentlandite, *Hz* heazlewoodite, *Ni* native nickel, *Cu* native copper published by Griffin et al. (2004) for similar low-temperature (< 1,100°C) Kaapvaal peridotite xenoliths and by Pearson et al. (2004) for a subset of peridotitic samples from the South-Eastern Terrane (Thaba Putsoa, Liqhobong, Matsoku). As noted by these authors, sulphur content does not correlate with $\mathrm{Fo}_{\mathrm{olivine}}$ or with other melt depletion indexes (Fig. 4a). The correlation between measured S contents and S contents calculated using BMS modal abundances is also very weak (Fig. 4b). The high S contents of the three Jagersfontein samples (140–155 ppm) are accounted for by sulphide clusters intergrown with Cr-spinel + clinopyroxene ± enstatite symplectites. The poorly reproducible S content of sample PHN 2899 (120–187 ppm; Table 2) testifies to a highly heterogeneous distribution of BMS. However, other S-rich samples do not contain any sulphides (e.g. KBD 4; Bult. 9; BG) or only one SI per polished thin section (BG2). This unbalanced S content may be explained by extremely small (< < 1 µm in diameter) sulphide particles dispersed throughout serpentinized veins or by kimberlite-related sulphates (cf. Griffin et al. 2004).

The four analysed PKP samples show rather reproducible high S contents (167–213 ppm), while their BMS modal abundances vary by a factor of 10 (Table 2). Image analysis of these samples likely overestimates BMS modal abundance because it takes into account Mt that extensively replaces intergranular sulphides (see below). This bias is superimposed on the highly heterogeneous distribution of BMS in PKP, which is also attested by the huge range in S concentration (80–2,055 ppm) published for 31 PKP samples from Bultfontein (Erlank et al. 1987).

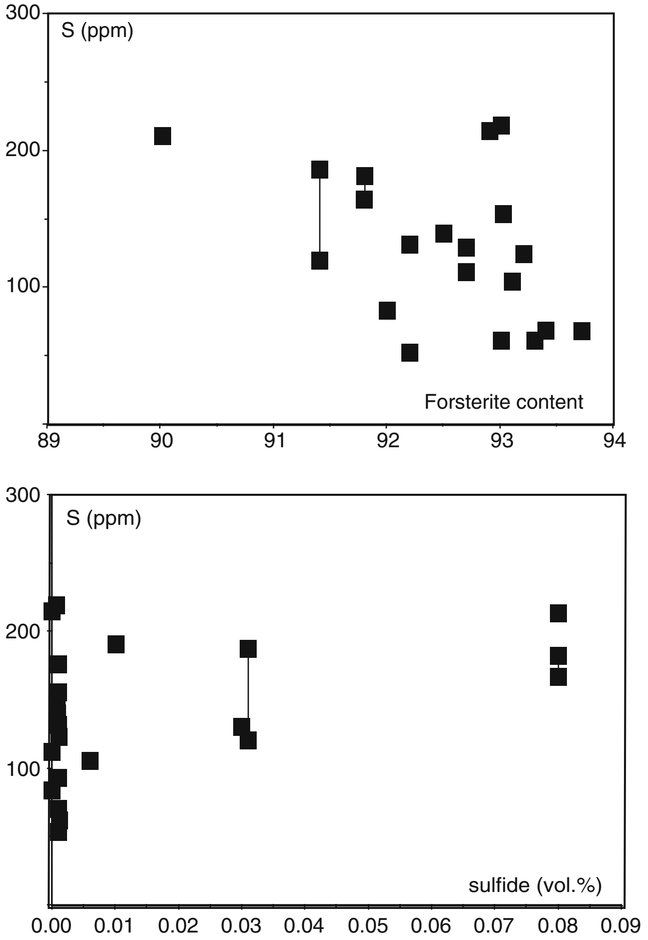

Fig. 4 Plot of bulk-rock S concentration vs Fo content of the olivine and estimated sulphide modal abundances. *PKP* Phlogopite-K-richterite peridotites

BMS assemblages

As in most mantle rocks, the sulphide mineral assemblages are not the same for inclusions in silicates and intergranular blebs. Unfractured SI are composed of finely intergrown pyrrhotite-like phases, a pinkish one and a greyish-blue one, which can be identified using oil immersion objectives (Fig. 2a). Electron microprobe analyses identify two Ni-rich pyrrhotite phases that plot inside the compositional field of monosulphide solid solution (Mss) in the Fe–Ni–S system (see below). They will be referred to as Mss 1 and Mss 2. Similar Mss phases have been widely reported in mantle samples entrained by alkali lavas (see Lorand and Conquéré 1983; Dromgoole and Pasteris 1987; Guo et al. 1999; Griffin et al. 2004 and reference therein). Mss 1 and Mss 2 usually occupy roughly a similar volume in a single inclusion except in LMA 18 and KBM 39 where Mss1 predominates over Mss 2, which is restricted as rare fine (1–5 µm thick) lath-like lamellae within Mss 1.

The other sulphides observed in the unfractured SI are pentlandite (Pn) and Cu-rich sulphides, i.e. chalcopyrite (Cp) or high-temperature solid solution (Iss). The Iss/Cp phases generally occur as thin discontinuous rims lining up the walls of the inclusion. Pn occurs as: (a) exsolved flames within the Mss phases, (b) coarser bodies at the periphery of the Mss (Fig. 2d). Modal proportions of each sulphide phase vary widely from one inclusion to another in a single xenolith. Three-phase assemblages Mss (1 + 2) + Iss/Cp or Mss (1 + 2) + Pn are common while four-phase assemblages Mss (1 + 2) + Iss/Cp + Pn are less abundant. As commonly observed in other mantle xenoliths, these grain-to-grain variations may be random artefacts of sectioning. On average, the Cu-rich sulphide phases fill less than 10% of the total volume of SI except in sample KBM 39 (10–20% Cu-sulphides). In this sample, one unfractured SI is devoid of Mss and displays coarse-grained Pn + Cp (Fig. 2e).

Fractured SI differ from unfractured SI by predominant Pn occurring as coarser flames isolating Mss blebs. In some cases, fine Pn rods cross-cut the Pn–Mss lamellar texture (Fig. 2f). Fractured SI surrounded by serpentinized fracture planes lack Mss: some inclusions preserve a rim of blocky Pn ± Iss/Cp, which is sometimes transformed into secondary Cu sulphides-chalcocite or digenite-like phases. The basal plane of the original Mss is filled with parallel serpentine fibers and Mt. Those SI that are completely coated by serpentine contain completely recrystallized sulphide assemblages consisting of massive Pn + Mt intergrowths (Mt; Fig. 2g). Pn is replaced by polycrystalline heazlewoodite (Hz) + Ni-bearing massive Mt in a few fractured inclusions from Bultfontein and Kimberley xenoliths. Native copper (Cu) is the Cu-rich phase in these Hz-bearing assemblages.

All the sulphide grains classified as intergranular (BMS occurrence 3) lack Mss and resemble fractured SI as regards their Cu–Fe–Ni mineral assemblages. The coarsest, regularly faceted grains (e.g. PHN 2899) are composed of massive Pn rims isolating a core of Pn flames; when they occur, Iss/Cp phases are systematically inside the Pn rim. Most of intergranular sulphides are now Hz + Pn + Mt ± Cu. Cu (and/or secondary sulphides, i.e. digenite) are very rare in magnesian peridotites ($Mg > 92$). A K–Fe–Cu phyllosulphide analogous to the mineral djerfisherite previously reported by Pasteris (1982) in kimberlite-hosted xenoliths is present in KBBJ 30 (Jagersfontein). Unfortunately, its grain size is too small to allow quantitative microprobe analysis. Intergranular sulphides in PKP, LMA 18 and KBM 39 are deeply transformed. Whereas unfractured SI have preserved Mss + Pn + Iss/Cp assemblages, almost all the fractured SI and intergranular grains consist of polycrystalline Hz, coexisting with Mt, Pn and secondary Cu-bearing minerals (Cu, digenite and chalcocite). Intergranular sulphides in PKP generally display a core of Hz + Pn almost completely replaced by microporous Mt (Fig. 2c). Cu and/or secondary Cu-sulphides are on average more abundant than in magnesian peridotites.

BMS in Jagersfontein and Bultfontein garnet-free peridotites systematically occur inside or in the vicinity of Cr-spinel + clinopyroxene + enstatite symplectites. Clinopyroxene may contain spherical SI. These BMS differ from the sulphide assemblages described above by a higher modal proportion of Hz which occurs either in the core of symplectitic intergrowths, as finely dispersed particles among myrmekitic chrome spinel (Fig. 2h) and in the sulphide veins that invade fracture planes and grain boundaries of the coarse-grained silicates surrounding the Cr-spinel + clinopyroxene ± enstatite symplectites. In some grains, Hz includes relict-like Pn + Mt intergrowths and/or euhedral skeletal Mt crystals (Fig. 2i). Native nickel displaying a characteristic bright silver colour, generally occurs as grains up to 300×100 μm^2 in size in olivine embayment adjacent to Cr-spinel + clinopyroxene ± enstatite symplectites, at some distance (although not far) from BMS (Fig. 2j); native Ni may also belong to these symplectites, being disseminated between vermicular pyroxenes. Relationships between native Ni and Hz are difficult to assess. However, in the few grains where they both coexist, native Ni is systematically rimmed by Hz.

Sulphide phase chemistry

The Mss compositions of unfractured SI plot in the stability field of synthetic Mss defined at 600°C by Kullerud et al. (1969) (Fig. 5). Most of the analyses of individual Mss were obtained from SI of the more fertile lherzolites, which are generally sulphide-rich, and contain the biggest Mss phases. Mss 2, the grey Mss phase, is richer in Ni and Co than Mss 1, the pink phase. Both are nearly devoid of Cu ($Cu < 0.05$ at.%) except in the vicinity of Cu-rich sulphides, where the electron beam may have drilled into the Cu sulphide. The two Mss phases exhibit variations in both their Ni/Fe and total metal/sulphur (M/S) ratios. EMP analyses yielding intermediate Ni/Fe ratios mostly reflect a beam overlap onto Mss 1–2 intergrowths at the micron to submicron scale during analysis (Table 3). Two olivine-hosted unfractured SI in samples BG2 and LMA 7 yield 17–21 at.% Ni, 0.2–0.4 at.% Co in Mss 2 vs. 11–14 at.% Ni, Co < 0.3 at.% in Mss 1. LMA 18 Mss phases display a broader compositional range (18–21 at.% Ni and up to 0.9 at.% Co in Mss 2 vs. 5.2–8 at.% Ni and < 0.1 at.% Co in Mss 2). Orthopyroxene-hosted SI contain higher proportions of Fe-rich Mss 1 (4.2–9.8 at.% Ni). Defocused-beam analyses in these samples yielded bulk compositions with intermediate Ni contents between the two Mss phases (13–17 at.% Ni; Table 3). In KBM 39, the most iron-rich lherzolite, the Mss 2 composition spans a larger range of Ni concentrations (15.8–20.9 at.% Ni), coupled with significant Co contents (up to 0.9 at.%). KBM 39 Mss 1 is always Ni-poor (4.2–9.8 at.% Ni), whether it occurs in olivine, orthopyroxene or clinopyroxene. Six defocused-beam EMP analyses of olivine-hosted and orthopyroxene-hosted inclusions in KBM 39 confirm the predominance of Mss 1 over Mss 2 (7.5–11.1 at.% Ni); these compositions plot on tie-lines connecting Pn and Mss 1 compositions, but very close to Mss 2 data points.

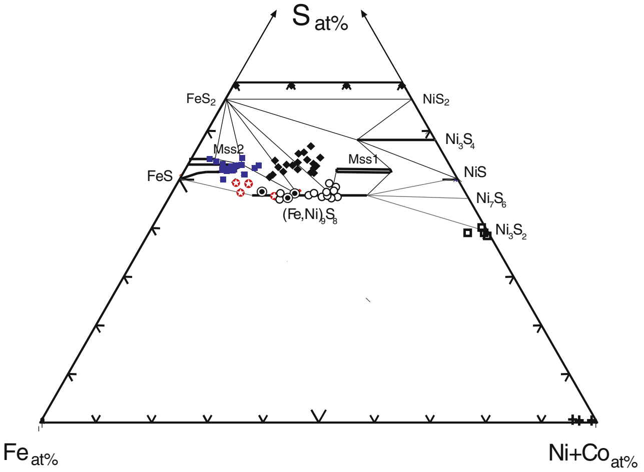

Fig. 5 Compositions of BMS from Kaapvaal peridotites in the Fe–Ni–S system at 250°C and atmospheric pressure. Phase relationships and Mss 1 and Mss 2 compositional fields after Craig (1973). *Closed diamonds*: high-Ni Mss; *filled squares*: low-Ni Mss; *stars*: euhedral SI containing rodlike Pn; *dotted circle*: fractured inclusions; *open circle*: Pn; *open squares*: Hz; *crosses*: native nickel. NiS_2: vaesite; FeS_2: Pyrite; NiS: Millerite; Ni_7S_6: godlevskite; Ni_3S_2: Hz

Table 3 Representative electron probe analyses of sulphide minerals from unfractured SI

Sample	BG2	Bult. 12			LMA 18			KBM 39				
	Bulk Mss	Mss 2	Mss1	Mss 2	Mss 1	Bulk Mss	Pn	Mss	Mss 2	Bulk Mss	Icb	Pn
wt%												
Fe	39.78	34.65	42.9	31.75	50.36	40.42	28.20	57.42	31.19	50.73	37.02	29.62
Ni	20.87	23.65	15.0	28.15	9.72	19.82	37.70	5.79	28.4	10.88	2.43	36.72
Co	0.15	0.27	0.62	0.1	0.43	0.35	0.18	1.00	0.10	0.10	0.06	0.45
Cu	–	–	0.04	–	0.12	–		–	0.11	–	22.74	–
S	39.64	40.3	39.2	39.40	39.2	38.60	33.70	35.97	39.86	38.42	37.49	32.43
Sum	100.94	99.2	97.4	99.98	99.8	99.54	99.95	99.40	99.66	100.20	99.74	99.21
Atom %												
Fe	31.55	27.03	34.15	24.84	39.4	31.80	22.50	45.65	24.16	39.58	29.76	24.38
Ni	15.00	17.58	11.32	20.96	7.2	14.83	28.34	4.38	20.86	8.08	1.91	28.76
Co	0.12	0.4	0.2	0.46	0.14	0.32	0.21	0.13	0.75	0.12	–	0.35
Cu	–	–	0.03	0.04	0.08	–	–	–	0.06	–	15.79	–
S	53.34	54.87	54.28	53.70	53.2	52.87	48.96	49.81	54.15	52.22	52.5	46.75

Mss 1 pink Mss, *Mss 2* greyish white Mss, *Bulk Mss* compositions obtained by defocused-beam analyses, *Pn* pentlandite, *Icb* isocubanite, – not detetected

The EMP data of rod-textured Pn/Mss intergrowth plot below the metal-rich boundary of the Mss stability field in the Fe–Ni–S system, reflecting a major contribution of the Pn (Fig. 5). Likewise, it was not possible to obtain reliable analyses of the Mss phases in the fractured inclusion because of their occurrence as thin lamellae within Pn. Pn associated with the two Mss phases in unfractured SI and the large euhedrally shaped intergranular Pn is Ni-rich ($0.79 < \mathrm{Fe/Ni_{at}} < 1.0$—Table 4). Such Pn compositions are usually found in pyrrhotite (hexagonal to monoclinic)–Pn assemblages (e.g. Misra and Fleet 1973; Lorand 1985, 1989a). Co content (0.2–0.5 at.%) increases in parallel with the Pn modal proportions. Pn in fractured inclusions or intergranular sulphides rimmed by serpentine minerals spans a large range of Fe/Ni ratio (0.81–1.59). The most Fe-rich Pn analyses ($\mathrm{Fe/Ni_{at}} = 1.59$) correspond to those from the Pn–Mt inclusions. The lowest Fe/Ni ratio (0.81) corresponds to the Pn relicts occurring inside Hz in fractured inclusions or intergranular sulphides from PKP samples. These Ni-rich Pns may be also significantly enriched in Co (up to 1.53 at.% Co).

Due to the small grain size, reliable analyses of Cu-sulphides were only obtained for four inclusions. In unfractured SI, the narrow rims of Cu sulphides around Mss phases consists of either isocubanite ($CuFe_2S_3$) or Cp. Cp was systematically found in Pn-rich grains, i.e. hexagonal-shaped SI, fractured inclusions and euhedral intergranular sulphides.

Heazlewoodite replacing Pn in fractured inclusions contains small amounts of Fe and Co (Table 4). It is a Fe-poor, stoichiometric Hz in BMS occurrences 3 and 4. Native nickel has a general formula ranging between $Ni_{0.95}$ $Fe_{0.05}$ and $Ni_{0.985}$ $Fe_{0.0089}$ $Cu_{0.0059}$.

Table 4 Representative electron probe analyses of opaque minerals in fractured SI and sulphide veins

Fractured inclusions					Sulphide veins				
Sample Mineral	BG2 Mss–Pn intergrowth	BG2 Pn	KBM 39 Pn	KBM 39 Cp	Bult. 6 Pn	Bult. 6 Hz	Bult. 4 Hz	Bult. 4 Ni	Bult. 4 Ni
wt%									
Fe	47.85	32.62	39.10	30.51	28.39	3.46	0.73	0.85	3.72
Ni	16.29	33.09	25.91	0.14	37.48	69.44	72.25	98.50	94.97
Co	0.37	0.92	0.48	0.03	0.16	0.16	–	–	0.05
Cu	–	0.23	0.48	32.92	0.24	0.24	–	0.59	0.38
S	34.45	33.12	32.85	34.82	32.79	26.64	27.59	0.01	–
Sum	98.96	99.98	98.82	98.42	99.48	100.32	100.61	100.71	99.20
Atom%									
Fe	38.63	26.55	32.09	25.37	23.79	2.97	0.62	0.89	3.93
Ni	12.53	25.62	20.22	0.11	29.25	56.63	58.47	98.5	95.59
Co	0.29	0.71	0.37	0.02	0.13	0.13	–	–	0.05
Cu	–	0.17	0.35	24.06	0.18	0.18	–	0.59	0.35
S	48.51	46.95	46.96	50.44	46.85	39.85	40.89	0.02	–

Cp chalcopyrite, *Hz* heazlewoodite, *Ni* native nickel
Other abbreviations as in Table 2

Discussion

Subsolidus re-equilibration: open vs closed system

The sulphide assemblage (Mss phases ± Pn ± isocubanite ± Cp) of unfractured SIs is typical of natural Ni–Cu sulphide ores quenched at high temperature. However, although kimberlites erupt at very high velocity (a few hours travel time from a depth >150 km; Spera 1987) kimberlite-hosted cratonic peridotite xenoliths (and diamonds) do not contain any sulphide paragenesis stable above 600°C. At this temperature, a unique Mss stability field straddles the central portion of the Fe–Ni–S system (Craig and Kullerud 1969; Vaughan and Craig 1978; Karup-Møller and Makovicky 1995 and reference therein; Fig. 5). Moreover, this Mss systematically contains Cu in solid solution (up to 1–2 wt% for 20–25 wt% Ni; Craig and Kullerud 1969; Czamanske and Moore 1977; Mac Queen 1979). The lack of detectable Cu content in Kaapvaal peridotite Mss demonstrates that they re-equilibrated at much lower temperature, i.e. long after their entrapment into silicates. The tie-line between Mss 1 (10 wt% Ni) and Cp is established at ca. 420°C (Craig and Kullerud 1969). Cooling experiments on synthetic sulphide assemblages in the Cu–Fe–Ni–S system suggest a breakdown into two discrete Mss phases at $T \leq 300°C$ (Craig 1973; Misra and Fleet 1973; Farell and Fleet 2002). Our Mss 1 composition agrees with that of Misra and Fleet (1973) and Craig (1973).

Pentlandite is stable below 610°C, and tie-lines between Mss and Pn are established at 590°C in the Cu–Fe–Ni–S system. The occurrence of Pn as small flames and coarser grains, sometimes within a single BMS grain, points to several exsolution temperatures (Kelly and Vaughan 1983). Between 600 and 300°C, the metal-rich side of the Mss stability field is progressively displaced towards more S-rich compositions, allowing Ni to be exsolved as Pn (Naldrett et al. 1967). In the Craig (1973) and Misra and Fleet (1973) experiments, the Mss 1 field evolves towards Fe-richer compositions when the temperature decreases below 300°C, whereas Mss 2 composition extends to ca. 21–22 at.% Ni (i.e. the Mss 2 composition of our samples LMA 18 and KBM 39) when temperature goes down to 200°C. Accordingly, the temperature of final equilibration of BMS in these two samples was around 200°C and the grain-by-grain variations in Ni content of the Mss 1 only reflect small differences between each SI.

Isothermal phase diagrams show that phase relationships in the central portion of the Fe–Ni–S system critically depend on the bulk M/S ratio, which is itself controlled by the fugacity of sulphur. Of course, any change of f_{S_2} at a given temperature modifies the sulphide assemblage. The subsolidus history discussed above assumes a constant M/S ratio in SI, i.e. that the fugacity of sulphur was internally buffered. It has long been demonstrated that sulphide assemblages disseminated in a volumetrically predominant silicate matrix are good indicators of the ambient redox conditions, and that the fugacity of sulphur deduced from those sulphide assemblages strictly reflects the oxygen fugacity imposed by the silicate assemblages (Eckstrand 1975; Eggler and Lorand 1993). In the mantle, the fugacity of sulphur is related to the fugacity of oxygen by the reaction:

$$2Fe_2SiO_{4(Ol)} + S_2 <=> 2FeS + Fe_2Si_2O_{6(Opx)} + O_2. \quad (1)$$

If applied to unfractured SI, the Eggler and Lorand (1993) calibration of equilibrium (1) yields sulphur fugacity between 0.5 and 3 and oxygen fugacity around FMQ to FMQ −2 log units at 950°C and $P = 4$ GPa, the average P–T conditions of equilibration of our Kaapvaal peridotites on a continental geotherm (Fig. 6). About 75% of the measured inclusions fit into this f_{O_2} range, which broadly agrees with that calculated for cratonic peridotites, although equilibrium (1) is by far less precise than equilibrium based on spinel or garnet (Daniels and Gurney 1991; Woodland and Koch 2003). The few outliers giving lower f_{O_2} and f_{S_2} are the Cu-sulphide rich inclusions from KBM 39; their high Cu-sulphide modal proportions increase the M/S ratios and thus decrease the f_{S_2} estimate. Three small inclusions give higher $f_{O_2} - f_{S_2}$ values, but in these cases, only defocused-beam EMP analyses were

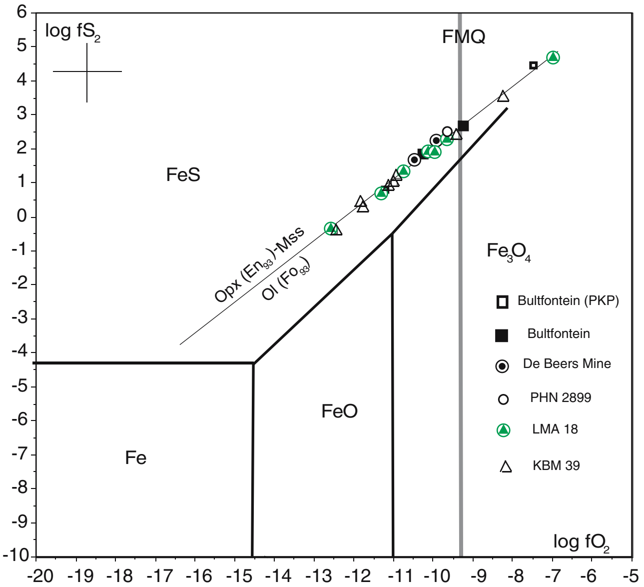

Fig. 6 $\log f_{O_2} - \log f_{S_2}$ diagram at 950°C, 4 GPa showing the range of $f_{S_2} - f_{O_2}$ conditions defined by the Mss compositions of unfractured inclusions. The thermodynamic database for the Fe–S–O system is from Robie et al. (1978) and Barton and Skinner (1979) extrapolated to 4 GPa by using volume terms of Kaufman (1963) and Scott (1973). The isopleths of iron atomic fraction in pyrrhotite (Toulmin and Barton 1964) have been extrapolated to 4 GPa by using the data from Eggler and Lorand (1993). The FMQ buffer curve is from Eggler and Lorand (1993) and was extrapolated to 4 GPa by using Wood (1987) and Scott (1973) integrated volume terms. Also shown is the olivine–enstatite–Mss curve for Fo_{93}, En_{93} and Mss Ni/Ni + Fe ratio of 0.3. Typical *error bars* are given on the upper left corner

performed. The $\log f_{S_2} - \log f_{O_2}$ diagram of Fig. 7 predicts that an isochemical re-equilibration down to 300°C under oxygen fugacity in the range FMQ to FMQ −2 log unit should produce a pyrrhotite-like phase ($Fe_{at} \leq 48\%$) coexisting with Ni-rich Pn (Ni/Fe molar ratio > 1). Since they contain such minerals, we can reasonably assume that our unfractured SI re-equilibrated in a closed system with respect to redox conditions.

There are at least two different interpretations of the Pn-rich BMS assemblages that occur in some euhedral SI, fractured SI and/or intergranular sulphides: (a) they are cooling products of the sulphide melt that coexists with the Mss from 996°C down to 862°C on the metal-rich side of the Fe–Ni–S system (Fig. 8) or (b) they are desulphurization products of Mss-rich assemblages. In theory, the metal-rich sulphide melt is progressively enriched in Ni when temperature decreases until the high-temperature Hz solid solution [$(Ni, Fe)_{3\pm x}S_2$] crystallizes at 862°C (Craig and Kullerud 1969). This latter synthetic mineral incorporates up to 30 at.% Fe at 725°C (Fig. 9): it produces massive Pn (plus minor amounts of low-Ni pyrrhotite) at a maximum *T* of 610°C by reacting with the coexisting Mss (Kullerud 1963). Rod-textured Pn may represent quenched textures from such high-*T* non-stoechiometric Hz. Literature data suggest some relationships between this type of texture and mantle peridotites that have reacted with volatile-rich small-degree melt fractions (Lorand and Conquéré 1983). It is also likely that the Cp–Pn two-phase BMS inclusion of sample KBM 39, a strongly metasomatized lherzolite, originated from a Ni-rich sulphide melt. Indeed, like Ni, Cu preferentially partitions into the sulphide melt with respect to the Mss (Fleet and Pan 1994; Li et al. 1996).

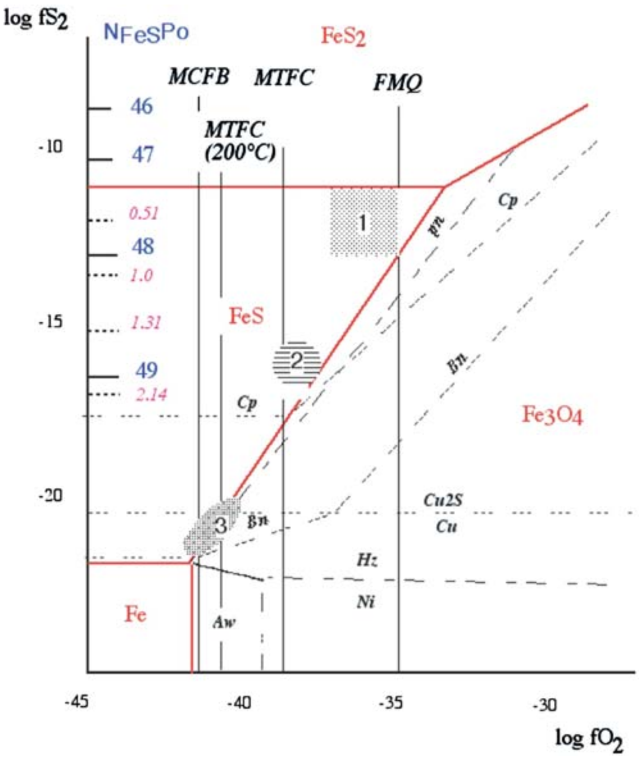

Fig. 7 $\log f_{O_2} - \log f_{S_2}$ diagram (300°C at athmospheric pressure), showing the redox conditions defined by: (1) unfractured SI, (2) fractured inclusions containing the assemblage Fe-rich Pn + Mt ± Po ± Cp), (3) fractured SI and intergranular sulphide showing the assemblage Pn + Hz + native Cu + Mt; thermodynamic database from Robie et al. (1978) and Barton and Skinner (1979) except for Pn (Cemic and Kleppa 1987); isopleths of iron atomic fraction in pyrrhotite and Fe/Ni in Pn are from Toulmin and Barton (1964) and Kaneda et al. (1986), respectively. The oxygen buffer assemblages are from Abrajano and Pasteris (1989). *Py* Pyrite; *Po* Pyrrhotite; *Fe* Native iron; *Mt* or *M* Magnetite; *Cp* Chalcopyrite; *Bo* Bornite; *Cc* Chalcocite; *Cu* Native copper; *Aw* Awaruite; *Ni* Native nickel; *Hz* Haezlewoodite; *C* Chrysotile; *F* Fayalite; *B* Brucite; *T* Talc

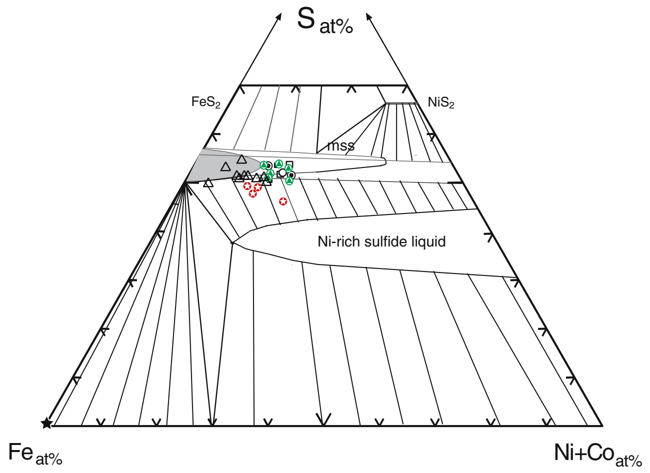

Fig. 8 Bulk compositions of unfractured SI in the Fe–Ni–S system (athmospheric pressure). Same symbols as in Fig. 5 except *stars*: euhedral SI containing rod-textured Pn exsolutions. Mss stability field at 1,100, 1,000 and 900°C after Craig and Kullerud (1969). Note that SI containing rod-like Pn exsolutions plot in the two-phase field domain Mss + Ni-rich sulphide liquid

By contrast, the fractured SI (and the intergranular sulphides) that differ from unfractured SI only by a much higher volume of Pn flames, while preserving the same lamellar microstructures, are assumed to have been desulphurized in the temperature range of the stability field of Pn (< 610°C). When desulphurized at constant Fe/Ni ratio and *T* below 610°C, bulk Mss compositions similar to those of SI exsolve more and more Pn with Fe/Ni ratios (molar) of 1.0–1.5 owing to the geometry of the Mss–Pn associations in the central portion of the Fe–Ni–S system (cf. Lorand and Conquéré 1983; Lorand 1989a). There is little doubt that this desulphurization sequence is related to serpentinization, as the BMS grains in question are commonly surrounded by serpentine minerals. Bishop et al. (1975) raised the possibility that the Pn + Mt intergrowths encountered in some Kimberley peridotite nodules crystallized from an oxygen-rich sulphide liquid. Our observations exclude such a magmatic origin because Pn + Mt intergrowths only occur in sulphide grains adjacent to serpentine veins, and because Mt encloses Cu, a typical serpentinization-derived opaque mineral. Moreover, Ni-rich mantle sulphide melts are not expected to crystallize much Fe-oxide because oxygen is poorly soluble in such melts at high pressure (<1 wt% at 3 GPa in the system Fe–S–O; Wendlandt and Huebner 1979; Cermer 1987; Brenan 2003).

The alteration sequence from unfractured SI to serpentinization-coated fractured SI and intergranular sulphides, i.e. Mss—Pn ± Mt—Hz and Iss—chalcocite–Cu, reflects the reducing conditions typically induced by an incipient serpentinization process affecting ultramafic rocks under water-deficient conditions (Lorand 1985, 1989a; Abrajano and Pasteris 1989). Fe-poor Hz is stable at T below 562°C (Kullerud et al. 1969). The occurrence of Hz + Ni-rich Pn as ultimate replacement products is consistent with the Ni-rich composition of the serpentinized olivine. The intergranular assemblage, Cu + Hz + Pn + Mt ± chalcocite points to low oxygen fugacity conditions compared to those calculated from unfractured SI (FMQ −5.5 log unit). Such reducing conditions could be produced at 300°C by the serpentinization-related paragenesis Mt + chrysotile + Fo + brucite or at 200°C by the paragenesis Mt + talc + Fo + chrysotile (Fig. 7). Lizardite- and brucite-bearing assemblages were reported in kimberlite-hosted ultramafic xenoliths (Mitchell 1989; Berg 1989). Thus, the BMS alteration sequence evidenced in the studied Kaapvaal xenoliths supports the hypothesis of a low-T serpentinization event that affected kimberlite-hosted xenoliths, perhaps involving surface water (cf. Mitchell 1989).

The Ni-rich opaque mineral assemblage (native Ni + Hz + Mt) that characterizes Cr-spinel + clinopyroxene ± enstatite symplectites deserves specific comments as: (a) it has been very rarely reported in terrestrial rocks and (b) its mode of formation remains debatable. Hz in this assemblage is a low temperature mineral because it includes serpentinization-derived euhedral Mt crystals and/or it replaces all the other observed opaque minerals including Pn. Likewise, a low-T origin seems to be logical for native Ni, which commonly occurs as single-phase interstitial grains coexisting with Hz. The few native nickel occurrences described so far in terrestrial rocks are all from serpentinized ultramafic rocks (e.g. Challis 1975). However, this interpretation does not explain why single-phase native Ni grains systematically occur in the olivine embayments resulting from the formation of Cr-spinel + clinopyroxene ± enstatite symplectites. We may speculate that symplectite formation allowed a Ni-excess in the system, which was not accommodated by symplectitic pyroxenes and Cr-spinel, thus liberating native Ni. Field and Haggerty (1994) calculated redox conditions suitable for native Ni to crystallize at 1,200°C and 2 GPa (from FMQ down to IW; Frost 1991). These authors interpreted such symplectites as stress-assisted decompression products from Al–Cr–Ca-rich clinoenstatite, which occurred prior to or during protokimberlite genesis and sampling. Obviously, native Ni would not have formed if some S were present at this stage. In the Fe–Ni–S system, native Ni and Hz cannot coexist above 625°C because a Ni-rich sulphide melt persists along the Ni–S join (Karup-Møller and Makovicky 1995; Fig. 9). The replacement texture of native Ni by Hz suggests a late S contamination, probably infiltrated from host kimberlites during their eruption stage. Note that at 300°C, the $f_{S_2} - f_{O_2}$ conditions defined by the assemblage Pn–Hz–Mt are outside the stability field of native Ni, thus making the latter metastable during the serpentinization process (Fig. 7).

Metasomatic vs residual origin of the sulphide phase

Variations of S abundances in Kaapvaal peridotite xenoliths have little relevance to mantle processes since they do not correlate with BMS modal abundances. All the discussion below will be centred on BMS textures and modal abundances. The sulphide blebs entrapped in mantle silicates originated from a sulphide melt that separated a Cu-rich sulphide melt after crystallization of Mss (e.g. Tsai et al.1979; Lorand and Conquéré 1983; Dromgoole and Pasteris 1987; Guo et al. 1999). The debate has recently focused on whether these blebs were trapped during partial melting event(s) or later introduced by "metasomatic" agents that triggered complete recrystallization of the major mantle silicates (Alard et al. 2000; Griffin et al. 2002, 2004; Lorand and Alard 2001). Fo contents of 93 ± 0.5 point to an average partial melting degree ≥30% for the most magnesian studied peridotites (Boyd 1989; Walker et al. 1989; Walter 1999; Herzberg 2005 and references therein). Whether sulphides could have survived to such high-degree of melting can be roughly estimated by a simple mass balance equation for batch melting (cf. Morgan 1986)

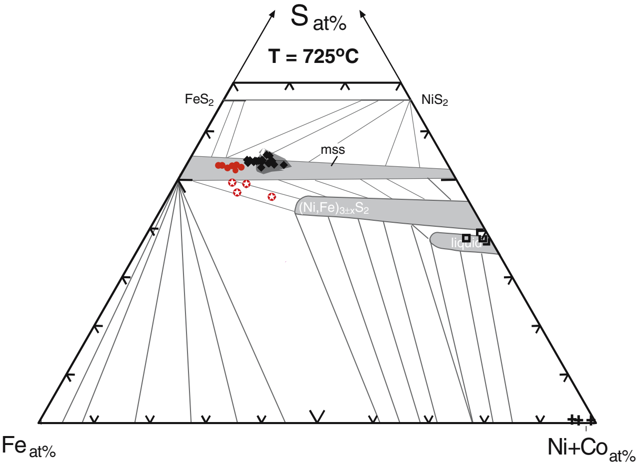

Fig. 9 Bulk compositions of Mss from samples LMA 18 and KBM 39 in the Fe–Ni–S system at 725°C and ambient pressure (after Karup-Møller and Makovicky 1995). *Filled diamond*: LMA 18; *closed circles*: KBM 39; *open stars*: euhedral SI containing rod-textured Pn exsolutions

$$C_R = (C_0 - FC_l)/(1 - F), \quad (2)$$

in which C_R is the sulphur content of the residue, C_0 the sulphur content of the mantle source, C_l the solubility of sulphur in the melt and F the melting degree, respectively. The primitive mantle S content (C_0), although still debated, is currently estimated at 250 ± 50 ppm (Lorand 1990; McDonough and Sun 1995 and reference therein). The melt resulting from $F = 30\%$ is expected to be ultramafic rather than basaltic. The sulphur content of such a silicate melt at sulphur saturation (C_l) was estimated to range from 1,600 to 2,700 ppm at $T = 1{,}450°C$ and $P = 1$ bar (Shima and Naldrett 1975) and from 3,370 to 3,760 ppm at $T = 1{,}500°C$ and $P = 1$ bar (Mavrogènes and O'Neill 1999). However, these authors experimentally demonstrated that the solubility of S in silicate melts strongly decreases at increasing pressure; for example the S melt content C_l could be as low as ca. 800 ± 200 ppm at $P = 5$ GPa. With this latter C_l value, residual sulphides could survive in partial melting residues (i.e. $C_R \geq 0$ ppm) for $F = 0.3$ and $C_0 = 250 \pm 50$ ppm, respectively. The main characteristics of residual sulphides are: (a) a high proportion of Mss subsolidus decomposition products because Mss is the most refractory sulphide in the mantle (e.g. Bockrath et al. 2004), (b) high and low concentrations in compatible PGEs (Os, Ir, Ru, Rh) and incompatible PGEs (Pt and Pd), respectively (Bulanova et al. 1996; Alard et al. 2000 and references therein). By using in-situ laser ICPMS and laser MC-ICPMS techniques, Griffin et al. (2004) concluded that sulphides displaying these two characteristics are common in Kaapvaal peridotite xenoliths. The fact that residual sulphides could have survived in strongly refractory cratonic mantle peridotites may be explained by the high pressures assumed for melting events in this tectonic setting. Indeed as discussed above, an increase of pressure decreases the solubility of sulphur in silicate melts and expands the Mss stability field relative to that of sulphide melt (Bockrath et al. 2004). Moreover, the extensive recrystallization of olivine and orthopyroxene in coarse-granular peridotites probably enhanced Mss entrapment.

The origin of sulphides in our most magnesian Kaapvaal peridotites cannot be firmly solved without in-situ PGE data. Nevertheless, some inferences can be drawn from the distribution coefficient of Ni and Fe between olivine and sulphide melt (Kd_3 of Fleet and McRae 1983). Although somewhat controversial at high oxygen fugacity, Kd_3 has been found to be rather constant (31; Brenan 2003 vs 28–35; Fleet 2001) over a wide range of sulphide melt NiS content under f_{O_2} conditions more reducing than FMQ −2 log unit. Kd_3's values have been calculated from bulk-compositions of unfractured SI for a set of nine studied peridotites (a detailed description of the olivine–sulphide Ni–Fe partitioning data is provided in the Electronic Supplementary Material). The few Kd_3 available for the most magnesian samples (10–12.6) are lower by a factor of 3 than those determined by experimental studies. In other words, the unfractured SIs are too low in Ni to have been in equilibrium with olivine at magmatic temperatures (i.e. 1,200–1,300°C). Pressure could probably not explain this discrepancy because diamond-hosted SI that display typical PGE pattern of residual sulphides give Kd_3 in the range of the experimental values (Bulanova et al. 1996). The unfractured SI may therefore represent a metasomatic sulphide phase trapped at subsolidus temperatures during episodic grain-growth of olivine and orthopyroxene. As discussed above, this interpretation is certainly also valid for the unfractured hexagonally shaped SI that mimic negative crystals and have M/S ratio >1 indicating entrapment of a significant proportion of Ni-rich sulphide melt, a characteristic feature of metasomatic sulphide components in mantle rocks (Alard et al. 2000; Lorand and Alard 2001; Luguet et al. 2003).

The metasomatic origin of sulphides occurring in the iron-enriched (Mg ≤ ca. 91.5) samples from the two studied Kaapvaal Terranes is less disputable because: (a) these samples display metasomatic petrogenetic features—either phlogopite alone, assemblages of phlogopite + K-richterite + titanate-like phases (PKP) or of phlogopite + ilmenite + rutile, features commonly associated with partial or complete recrystallization of the main anhydrous silicates, (b) in addition to being sulphide-rich, the samples contain a high proportion of intergranular sulphides and (c) SI are observed in both anhydrous (clinopyroxene) and hydrous metasomatic phases (phlogopite) as well as in olivine neoblasts surrounding intergranular sulphides, clearly indicating secondary entrapment of sulphide melt during solid-state recrystallization. The studied Kaapvaal peridotites evidence two sulphide precipitation mechanisms—from fluids and from melts, respectively.

The potassium-rich metasomatism that generated PKP xenoliths is ascribed to H_2O-rich fluids or melts (perhaps related to kimberlites) that infiltrated the mantle at $T = 900–1{,}100°C$ and $P = 2–3$ GPa (Erlank et al. 1987; Haggerty 1991; Kinny et al. 1993; Grégoire et al. 2002). Sulphides may precipitate from a fluid phase via sulphidation reactions with silicates (Ballhaus and Stumpfl 1986). In the reducing conditions determined for cratonic mantle peridotites, S is assumed to partition into fluids as H_2S rather than SO_2 (Eggler and Lorand 1993; Woodland and Koch 2003). Thus, sulphidation reactions can be schematically written as

$$H_2S_{(V)} + FeO,\ NiO_{(S)} \rightarrow Mss + H_2O_{(V)}, \quad (3)$$

where V is the vapor phase, S a silicate and Mss a Fe–Ni monosulphide solution. Thin sulphide rims around phlogopite crystals evidence such sulphidation reactions. Although strongly modified during late low-T serpentinization, the metasomatic sulphide assemblages of PKP xenoliths are poor in Cu-rich minerals, reflecting the very low Cu content (compared to Ni and Fe) of the silicates involved in the reaction process.

There are several features, which indicate that the enrichment in sulphide observed in the less magnesian xenoliths from the Southeastern Kaapvaal Terrane is related to sulphide melt(s). The spherical (or negative in orthopyroxene) crystal shape of most of the SI observed in samples LMA 18 and KBM 39 indicates entrapment of sulphide melt. Iron–titanium mantle metasomatism is commonly related to silicate melt because only such types of melts can transport the Ti allowing ilmenite to crystallize (Menzies et al. 1987). The metasomatic mineral assemblage rutile, ilmenite, phlogopite and sulphides (IRPS) was previously related to the infiltration of the Matsoku garnet peridotites by such a Ti-rich melt (Harte et al. 1975, 1987). Samples KBM 39 and LMA 18 differ from the IRPS suite of samples by a higher modal proportion of SI with respect to intergranular sulphides. Only a pervasive melt infiltration associated with extensive recrystallization of the silicate matrix may explain the widespread dispersion of SI in all of the silicate minerals (including clinopyroxene and garnet) as well as the fact that SI may occur as clusters of inclusions in a single crystal. In both samples LMA 18 and KBM 39, the estimated Kd_3 (5.1–13.8, but one value at 16.8) are far from the range of equilibrium value of 30–35. This range and the high proportion of Cu-sulphides enclosed in KBM 39 are more consistent with pyroxenitic lithologies (Shaw 1997; Zajacs and Szabo 2003) and support the hypothesis that the sulphides now encapsulated in anhydrous mantle silicates originally segregated from an exotic mafic melt.

Sulphide clusters associated with Cr-spinel + clinopyroxene + enstatite symplectites emphasize a third major possibility of S contamination in kimberlite-hosted mantle xenoliths, i.e. during protokimberlite genesis and sampling. The potential of kimberlitic magmas to contaminate mantle xenoliths with sulphides was suggested by earlier workers (e.g. Frick 1973) and is supported by the occurrence of BMS in kimberlites, either enclosed in olivine phenocrysts or as pyrrhotite in the mesostasis (Stone et al. 1989). However, this S contamination would have to occur during decompression of the xenoliths within the mantle in order to explain the preferential precipitation of sulphides inside symplectitic minerals. It is interesting to note that, although serpentinization deeply obliterates the initial mineralogy of sulphide clusters and sulphide veins, no Cu-rich opaque mineral has been identified in sulphide clusters associated with Cr-spinel + clinopyroxene ± enstatite symplectites. Therefore, the sulphur transport likely involved vapor S rather than immiscible sulphide melts which are expected to crystallize variable amount of Cu-sulphide during cooling.

Conclusion

Mantle-derived BMS indicate a strong effect of the serpentinization in Kaapvaal peridotite xenoliths. Compared to Mss-rich unfractured inclusions, the opaque mineral assemblages of both fractured inclusions and intergranular BMS point to a progressive desulphurization by serpentinization-related fluids. This trend is consistent with the reducing conditions generated by low-temperature retrogressive serpentinization.

Although not unlikely, the occurrence of Mss of residual origin in the most refractory studied peridotite xenoliths is difficult to reconcile with the estimated Kd_3 values that are too low for an equilibrium with olivine at magmatic temperature. The Pn-rich euhedral SI may have crystallized from a more metal-rich sulphide melt than Mss.

The inverse relationships between mantle-derived BMS modal abundances and olivine Fo content in Kaapvaal peridotites cannot be interpreted as a mantle melting trend because BMS in the less refractory peridotites show all characteristic features of a metasomatic origin. At least two BMS precipitation processes can be recognized: (1) precipitation from Fe–Cu-rich immiscible sulphide melts in phlogopite-(ilmenite–rutile) peridotites and (2) sulphidation reactions from an H_2S-rich fluid phase for PKP samples.

The whole-rock S contents may be misleading for evaluating the S concentration range of the cratonic SCLM. The same conclusion emerged from the study of basalt-hosted mantle xenoliths, based on the observations that BMS are usually strongly weathered (e.g. Lorand 1990). Unlike basalt-hosted peridotite xenoliths, Kaapvaal kimberlitic mantle xenoliths display weaker weathering evidence. Contamination by kimberlitic magmas during the decompression of the xenoliths within the mantle and then by crustal fluids during serpentinization process, account for the disturbance of whole-rock S abundances.

Acknowledgements The authors thank Adolphe Nicolas for the South Eastern Terrane samples, Michel Fialin (Camparis, University "Pierre et Marie Curie") for his assistance with electron microprobe analyses and Michel Gros for bulk-rock S analyses. Financial supports were provided by CNRS (FRE 2456 and UMR 7160). Constructive reviews and comments made by W.L. Griffin, an anonymous reviewer and the executive editor T. Grove helped to improve the paper and are highly appreciated.

References

Abrajano T, Pasteris JD (1989) Zambales ophiolite, Philippines II. Sulfide petrology of the critical zone of the Acoje massif. Contrib Mineral Petrol 103:64–77

Alard O, Griffin WL, Lorand JP, Pearson N, O'Reilly SY (2000) Non-chondritic HSE patterns in mantle sulfides. Nature 407:891–894

Alard O, Griffin WL, Pearson N, Lorand JP, O'Reilly SY (2002) New insights into the Re-Os systematics of sub-continental lithospheric mantle from in-situ analyses of sulfides. Earth Planet Sci Lett 203:651–663

Andersen T, Griffin W, O'Reilly SA (1987) Primary sulphide melt inclusions in mantle-derived megacrysts and pyroxenites. Lithos 20:279–95

Aulbach S, Griffin WL, Pearson NJ, O'Reilly SY, Kivi K, Doyle BD (2004) Mantle formation and evolution, slave craton. Constraints from HSE abundances and Re–Os isotopes. In: Reisberg L, Lorand J-P, Alard O, Ohnenstetter M (eds) Highly siderophile elements and igneous processes. Chem Geol 208:61–88

Ballhaus C, Stumpfl EG (1986) Sulfide and platinum mineralization in the merensky reef: evidence from hydrous silicates and fluid inclusions. Contrib Mineral Petrol 94:93–204

Barton PB, Skinner BJ (1979) Sulfide minerals stabilities. In: Barnes HL (ed) Geochemistry of hydrothermal ore deposits. Holt Rinehart and Winston, New York, pp 236–333

Berg GW (1989) The significance of brucite in South African kimberlites. In: Ross J, Jaques AL, Ferguson J, Green DH, O'Reilly SY, Danchin RV, Janse AJA (eds) Kimberlites and related rocks. Their composition occurrence origin and emplacement. vol 1. GSA Spec Publ No 14, Blackwell, Oxford, pp 7–45

Bishop FC, Smith JV, Dawson JB (1975) Pentlandite magnetite intergrowth in De beers spinel lherzolite: review of sulfides in nodules. Phys Chem Earth 9:323–337

Bockrath C, Ballhaus C, Holsheid A (2004) Fractionation of the platinum-group elements during mantle melting. Science 305:1951–1953

Boyd FR (1989) Compositional distinction between oceanic and continental lithosphere. Earth Planet Sci Lett 96:15–26

Boyd FR, Gurney JJ (1986) Diamonds and the Archean lithosphere. Science 232:472–477

Boyd FR, Nixon PH (1978) Ultramafic nodules from the Kimberley pipes, South Africa. Geochim Cosmochim Acta 42:1367–1382

Brenan J (2003) Effects of f_{O_2}, f_{S_2}, temperature, and melt composition on Fe–Ni exchange between olivine and sulfide liquid: implications for natural olivine–sulfide assemblages. Geochim Cosmochim Acta 67:2663–2681

Brey GP, Köhler T (1990) Geothermobarometry in four-phase lherzolites. II. New thermobarometers, and practical assessment of existing thermobarometers. J Petrol 31:1353–1378

Bulanova GP, Griffin WL, Ryan CG, Shestakova Ye O, Barnes SJ (1996) Trace elements in sulfide inclusion from Yakutian diamonds. Contrib Mineral Petrol 124:111–125

Cemic L, Kleppa OJ (1987) High temperature calorimetry of sulphide systems. II: standard enthalpies of formation of pentlandite and violarite. Phys Chem Miner 14:52–57

Cermer RS (1987) The distribution of minor elements in nickel matte smelting. Unpublished PhD thesis, University of Toronto, 341 pp

Challis GA (1975) Native nickel from the Jerry River, South Westland, New Zealand; an example of natural refining, Miner Mag 40:247–251

Craig JR (1973) Pyrite-pentlandite assemblages in the Fe–Ni–S system. Am J Sci 273A:496–510

Craig JR, Kullerud G (1969) Phase relations in the Cu–Fe–Ni–S system and their applications to magmatic ore deposits. In: magmatic ore deposits. Econ Geol Monogr 4:343–358

Czamanske GK, Moore JB (1977) Composition and phase chemistry of sulfide globules in basalt from the Mid-Atlantic ridge rift valley near 37°N lat. Geol Soc Am Bull 88:587–599

Daniels LRM, Gurney JJ (1991) Oxygen fugacity constraints on the southern African lithosphere. Contrib Mineral Petrol 108:154–161

Dawson JB, Smith JV, Hervig RL (1980) Heterogeneity in upper mantle lherzolite and harzburgites. Philos Trans R Soc Lond A 297:323–331

De Wit MJ, Roering Ch, Hart RG, Armstrong RA, De Ronde CEG, Green RWE, Tredoux M, Peberdy E, Hart RA (1992) Formation of an Archean continent. Nature 357:553–562

Desborough AT, Czamanske GK (1973) Sulfides in eclogite nodules from a kimberlite pipe, South Africa, with comments on violarite stoechiometry. Am Mineral 58:195–202

Dromgoole EL, Pasteris JD (1987) Interpretation of the sulfide assemblages in a suite of xenoliths from Kilbourne Hole, New Mexico. Geol Soc Am Spec Pap 215:25–45

Eckstrand OR (1975) The Dumont serpentinite: a model for control of nickeliferous opaque mineral assemblages by alteration reactions in ultramafic rocks. Econ Geol 70:183–201

Eggler DH, Lorand JP (1993) Mantle sulfide oxybarometry. Geochim Cosmochim Acta 57:2213–2222

Erlank AJ, Waters FG, Hawkesworth CJ, Haggerty SE, Allsopp HL, Rickard RS, Menzies MA (1987) Evidence for mantle metasomatism in peridotite nodules from the kimberley pipes, South Africa. In: Menzies MA, Hawkesworth CJ (eds) Mantle metasomatism. Academic, London, pp 226–309

Farell SP, Fleet ME (2002) Phase separation in (Fe, Co)$_{1-x}$S monosulfide solid-solution below 450°C, with consequences for coexisting pyrrhotite and pentlandite in magmatic sulfide deposits. Can Mineral 40:33–46

Field SW, Haggerty SE (1994) Symplectites in upper mantle peridotites; development and implications for the growth of subsolidus garnet, pyroxene and spinel. Contrib Mineral Petrol 118:138–156

Fleet ME (2001) A comment on Fe–Ni exchange between olivine and sulphide liquid: implications for oxygen barometry in sulphide saturated magmas by Brenan and Caciagli (2000). Geochim Cosmochim Acta 65:4425–4427

Fleet ME, MacRae ND (1983) Partition of Ni between olivine and sulfide and its application to Ni–Cu sulfide deposits. Contrib Mineral Petrol 83:75–81

Fleet ME, Pan Y (1994) Fractional crystallization of anhydrous sulfide melt in the system Fe–Ni–Cu–S, with application to magmatic sulfide deposits. Geochim Cosmochim Acta 58:3369–3377

Frick C (1973) Sulfides in griquaite and garnet peridotite xenoliths in kimberlite. Contrib Mineral Petrol 39:1–16

Frost RB (1991) Introduction to oxygen fugacity and its petrological importance. In: Ribbe PH (ed) Reviews in mineralogy, vol 25. Mineral Soc Am, pp 1–9

Grégoire M, Bell DR, Le Roex AP (2002) Trace element geochemistry of phlogopite-rich mafic mantle xenoliths: their classification and their relationship to phlogopite-bearing peridotites and kimberlites revisited. Contrib Mineral Petrol 142:603–625

Grégoire M, Bell DR, Le Roex AP (2003) Garnet lherzolites from the Kaapvaal craton (South Africa): trace element evidence for a metasomatic history. J Petrol 44:629–657

Griffin WL, O'Reilly SY, Natapov LM, Ryan CG (2003a) The evolution of lithospheric mantle beneath the Kalahari Craton and its margins. Lithos 71:215–241

Griffin WL, O'Reilly SY, Abe N, Aulbach S, Davies RM, Pearson NJ, Doyle BJ, Kivi K (2003b) The origin and evolution of Archean lithospheric mantle. Precambrian Res 127:19–41

Griffin WL, Spetsius ZV, Pearson NJ, O'Reilly SY (2002) In situ Re–Os analysis of sulfide inclusions in kimberlitic olivine: new constraints on depletion events in the Siberian lithospheric mantle. Geochem Geophys Geosyst 3:1069; doi:10.1029/2001GC000287

Griffin WL, Graham S, O'Reilly SY, Pearson NJ (2004) Lithosphere evolution beneath the Kaapvaal Craton: Re–Os systematics of sulfides in mantle-derived peridotites. In: Reisberg L, Lorand J-P, Alard O, Ohnenstetter M (eds) Highly siderophile elements and igneous processes. Chem Geol 208:95–215

Gros M, Lorand JP, Bezos A (2005) Determination of total sulfur contents in international rock standard SY-2 and other mafic and ultramafic rocks using an improved scheme of combustion/iodometric titration. Geoanal Geostand Newslett 29:123–130

Guo J, Griffin WL, O'Reilly SY (1999) Geochemistry and origin of sulfide minerals in mantle xenoliths: Qilin, Southeastern China. J Petrol 40:1125–1151

Gurney JJ (1989) Diamonds. In: Ross J, Jaques AL, Ferguson J, Green DH, O'Reilly SY, Danchin RV, Janse AJA (eds) Kimberlites and related rocks. Their mantle/crust setting. Diamonds and diamonds exploration, vol 2. GSA Spec Publ No 14, Blackwell, Oxford, pp 935–966

Gurney JJ, Harte B, Cox KG (1975) Mantle xenoliths in the Matsoku kimberlite pipes. Phys Chem Earth 9:507–523

Haggerty SE (1989) Upper mantle opaque mineral stratigraphy and the genesis of metasomites and alkali-rich melts. In: Ross J, Jaques AL, Ferguson J Green DH, O'Reilly SY, Danchin RV, Janse AJA (eds) Kimberlites and related rocks. Their mantle/crust setting. Diamonds and diamonds exploration, vol 2. GSA Spec Publ No 14, Blackwell, Oxford, pp 687–700

Haggerty SE (1991) Oxide mineralogy of the upper mantle. In: Lindsley DH (ed) Oxide minerals: petrologic and magnetic significance. Rev Mineral 25:335–416

Harley SL (1984) An experimental study of the partitioning of Fe and Mg between garnet and orthopyroxene. Contrib Mineral Petrol 86:359–373

Harte B, Cox KG, Gurney JJ (1975) Petrography and geological history of upper mantle xenoliths from the Matsoku kimberlite pipe. In: Ahrens LH, Dawson JB, Duncan AR, Erlank AJ (eds). Phys Chem Earth 9:447–606

Harte B, Hawkesworth CJ (1989) Mantle domains and mantle xenoliths. In: Ross J, Jaques AL, Ferguson J, Green DH, O'Reilly SY, Danchin RV, Janse AJA (eds) Kimberlites and related rocks, vol 2: their mantle/crust setting. Diamonds and diamonds exploration. GSA Special Publication No 14, Blackwell, Oxford, pp 649–687

Harte B, Winterburn P, Gurney JJ (1987) Metasomatic and enrichment phenomena in garnet peridotite facies mantle xenoliths from the Matsoku kimberlite pipe, Lesotho. In: Menzies MA, Hawkesworth CJ (eds) Mantle metasomatism. Academic Press, London, pp 145–220

Herzberg CT (2005) Geodynamic information in peridotite petrology. J Petrol 45:2507–2530

Hops JJ, Gurney JJ, Harte B, Winterburn (1989) Megacrysts and high temperature nodules from the Jagersfontein kimberlite pipe. In: Ross J, Jaques AL, Ferguson J, Green DH, O'Reilly SY, Danchin RV, Janse AJA (eds) Kimberlites and related rocks. Their mantle/crust setting. Diamonds and diamonds exploration, vol 2. GSA Special Publication No 14, Blackwell, Oxford, pp 759–770

Kaneda H, Takenouchi S, Shoji T (1986) Stability of pentlandite in the Fe–Ni–Co–S system. Mineral Deposit 21:169–181

Karup-Møller S, Makovicky E (1995) The phase system Fe–Ni–S at 725°C. Neues Jahrb Mineral Monatsh 26:1–10

Kaufman L (1963) Phase equilibria and transformations in metals under pressure. In: Paul W, Warshauer DR (eds) Solids under pressure. McGraw Hill, New York, pp 304–355

Kelly DP, Vaughan DJ (1983) Pyrrhotine-pentlandite ore textures: a mechanistic approach. Mineral Mag 47:453–463

Kinny PD, Harte B, Graham CM (1993) Trace-element and D/H isotopic analyses of minerals from metasomatized mantle peridotite xenoliths. Terra Abstract, pp 373 [abstract]

Kullerud G (1963) Thermal stability of pentlandite. Can Mineral 7:353–366

Kullerud G, Yund RA, Moh G (1969) Phase relations in the Cu–Fe–S, Cu–Ni–S and Fe–Ni–S systems. In: Wilson HDB (ed) Magmatic ore deposits. Monog Econ Geol 4:323–343

Li C, Barnes S-J, Maskovicky E, Rose-Hansen J, Makovicky M (1996) Partitioning of nickel, copper, iridium, rhenium, platinum and palladium between monosulfide solid solution and sulfide liquid: effects of composition and temperature. Geochim Cosmochim Acta 60:1231–1238

Lorand JP (1985) The behaviour of the upper mantle sulfide component during the incipient serpentinization of alpine-type peridotites as exemplified by the Beni Bousera (Northern Morocco) and Ronda (Southern Spain) ultramafic bodies. Tschermak Mineral Petrogr Mitt 34:183–209

Lorand JP (1989a) Mineralogy and chemistry of Cu–Fe–Ni sulfides in mantle-derived spinel peridotite bodies from Ariège (Northeastern Pyrenees, France). Contrib Mineral Petrol 103:335–345

Lorand JP (1989b) Abundance and distribution of Cu–Fe–Ni sulfides, sulfur, copper and platinum-group elements in orogenic-type spinel peridotites of Ariège (Northeastern Pyrenees, France). Earth Planet Sci Lett 93:50–64

Lorand JP (1990) Are spinel lherzolite xenoliths representative of the sulfur content of the upper mantle? Geochim Cosmochim Acta 54:1487–1493

Lorand JP, Alard O (2001) Geochemistry of platinum-group elements in the sub-continental lithospheric mantle; in-situ and whole-rock analyses of some spinel peridotite xenoliths, Massif Central, France. Geochim Cosmochim Acta 65:2789–2806

Lorand JP, Conquéré F (1983) Contribution à l'étude des sulfures dans les enclaves de lherzolite à spinelle des basaltes alcalins (Massif Central et Languedoc, France). Bull Minéral 106:585–606

Lorand JP, Alard O, Luguet A, Keays RR (2003) S/Se systematics of the sub-continental lithospheric mantle beneath the Massif Central. Geochim Cosmochim Acta 67:4137–4153

Lorand JP, Delpech G, Grégoire M, Moine B, O'Reilly SY, Cottin JY (2004) Highly siderophile elements and the multi-stage metasomatic history of Kerguelen lithospheric mantle (south Indian ocean). In: Reisberg L, Lorand J-P, Alard O, Ohnenstetter M (eds) Highly siderophile elements and igneous processes. Chem Geol 208:195–215

Luguet A, Lorand JP, Seyler M (2003) A coupled study of sulfide petrology and highly siderophile element geochemistry in abyssal peridotites from the Kane fracture zone (MARK area, Mid-Atlantic ridge). Geochim Cosmochim Acta 67:1553–1570

Mac Queen KG (1979) Experimental heating and diffusion effects in the Fe–Ni–S ore from Redross, Western Australia. Econ Geol 74:140–148

Mavrogènes JA, O'Neill HSC (1999) The relative effects of pressure, temperature and oxygen fugacity on the solubility of sulfide in mafic magmas. Geochim Cosmochim Acta 63:1173–1180

McDonough WF, Sun SS (1995) The composition of the earth. Chem Geol 120:223–253

Menzies MA, Rogers N, Tindle A, Hawkesworth CJ (1987) Metasomatic and enrichment processes in lithospheric peridotites, an effect of asthenosphere-lithosphere interaction. In: Menzies MA, Hawkesworth CJ (eds) Mantle metasomatism. Academic, London, pp 313–361

Meyer HOA, Boctor NZ (1975) Sulfide oxide minerals in eclogite from Stockdale kimberlite, Kansas. Contrib Mineral Petrol 52:57–68

Misra K, Fleet ME (1973) The chemical composition of synthetic and natural pentlandite assemblages. Econ Geol 68:518–539

Mitchell RH (1989) Aspects of the petrology of kimberlites and lamproites: some definitions and distinctions. In: Ross J, Jaques AL, Ferguson J, Green DH, O'Reilly SY, Danchin RV, Janse AJA (eds) Kimberlites and related rocks. Their composition, occurrence, origin and emplacement, vol 1. GSA Spec Publ No 14, Blackwell, Oxford, pp 7–45

Morgan JW (1986) Ultramafic xenoliths; clue to the earth's late accretionary history. J Geophys Res 91:12375–12387

Naldrett AJ, Craig JR, Kullerud G (1967) The central portion of the Fe–Ni–S system and its bearing on pentlandite exsolution in iron-nickel sulfides ores. Econ Geol 62:826–847

Nixon PH (1987) Mantle Xenoliths. Wiley, Chichester

Pasteris JD (1982) Evidence of potassium metasomatism in mantle xenoliths: EOS Transactions [abstract]. Am Geophys Union 63:462

Pattou L, Lorand JP, Gros M (1996) Non-chondritic PGE ratios in the terrestrial upper mantle. Nature 379:712–715

Pearson DG, Irvine GJ, Ionov DA, Boyd FR, Dreibus GE (2004) Re–Os isotope systematics and platinum group element fractionation during mantle melt extraction: a study of massif and xenolith peridotite suites. In: Reisberg L, Lorand J-P, Alard P, Ohnenstetter (eds) Highly siderophile elements and igneous processes. Chem Geol 208:29–58

Robie RA, Hemingway BJ, Fisher JR (1978) Thermodynamic properties of minerals and related substances at 298.15 K and 1 bar (10^5 pascals) pressure and at higher temperatures. US Geol Surv Bull 1452:456

Shaw CSJ (1997) Origin of sulfide blebs in variably metasomatised mantle xenoliths, quaternary West Eifel volcanic field, Germany. Can Mineral 35:1453–1463

Shima H, Naldrett AJ (1975) Solubility of sulfur in an ultramafic melt and the relevance of the system Fe–S–O. Econ Geol 70:960–967

Sobolev NV, Lavren'Yev Yu G, Pokhilenko NP, Usova LV (1973) Chrome-rich garnets from the kimberlites of Yakutia and their paragenesis. Contrib Mineral Petrol 40:39–52

Spera F (1987) Dynamic of translithospheric migration of metasomatic fluid and alkaline magma. In: Menzies MA, Hawkesworth CJ (eds) Mantle metasomatism. Academic Press, London, pp 1–18

Stone WE, Fleet ME, Mac Rae ND (1989) Two-phase nickeliferous monosulfide solid solution (mss) in megacrysts from Mount Shasta, California: a natural laboratory for nickel-copper sulfides. Am Mineral 74:981–993

Taylor WR (1998) An experimental test of some geothermometer and geobarometer formulations for upper mantle peridotites with application to the thermobarometry of fertile lherzolite and garnet websterite. N Jahrb Mineral Abh 172:381–408

Toulmin P, Barton PB (1964) A thermodynamic study of pyrite and pyrrhotite. Geochim Cosmochim Acta 68:641–671

Tsai YN, Shieh NH, Meyer HOA (1979) Mineralogy and $^{34}S/^{32}S$ ratios of sulfides associated with kimberlites, xenoliths and diamonds. In: Boyd FR, Meyer HOA (eds) The mantle sample: inclusions in Kimberlites and other volcanics. Proceedings of the second international kimberlite conference, vol 2, pp 87–103

Vaughan DJ, Craig JR (1978) Mineral chemistry of metal sulfides. Cambridge University Press, Cambridge, pp 493

Walker RJ, Carlson RW, Shirey SB, Boyd FR (1989) Os, Sr, Nd, and Pb isotope systematics of southern African peridotite xenoliths: implications for the chemical evolution of sub-continental mantle. Geochim Cosmochim Acta 53:1583–1595

Walter MJ (1999) Melting residues of fertile peridotite and the origin of cratonic lithosphere. In: Fei Y, Betka C, Mysen BO (eds) Mantle petrology: field observations and high pressure experimentation, vol 6. The Geochemical Society, Houston, pp 225–240

Wendlandt RF, Huebner JS (1979) Melting relations of portions of the system Fe–S–O at high pressures and applications to the composition of the earth's core (abstr.) Lunar and Planetary Science X, Lunar and Planetary Institute, Houston, 1329–1331

Woodland AB, Koch M (2003) Variation in oxygen fugacity with depth in the upper mantle beneath the Kaapvaal craton, Southern Africa. Earth Planet Sci Lett 214:295–310

Zajacs Z, Szabo C (2003) Origin of sulfide inclusions in cumulate xenoliths from Nögrad-Gömör volcanic field, Pannonian Basin (North Hungary, South Slovakia). Chem Geol 194:105–117